Intramontane basin development related to contractional and extensional structure interaction at the termination of a major sinistral fault: the Húercal-Overa Basin (Eastern Betic Cordillera)

Antonio Pedrera, Jesús Galindo-Zaldívar, Alejandro Tello, Carlos Marín-Lechado

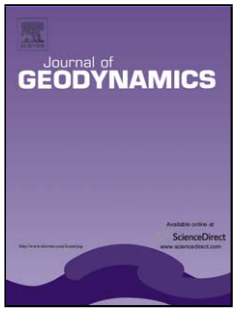

Title: Intramontane basin development related to contractional and extensional structure interaction at the termination of a major sinistral fault: the Húercal-Overa Basin (Eastern Betic Cordillera)

Authors: Antonio Pedrera, Jesús Galindo-Zaldívar, Alejandro Tello, Carlos Marín-Lechado

PII: S0264-3707(10)00021-9
DOI: doi:10.1016/j.jog.2010.01.008
Reference: GEOD 971

To appear in: *Journal of Geodynamics*

Received date: 17-9-2009
Revised date: 8-1-2010
Accepted date: 8-1-2010

Please cite this article as: Pedrera, A., Galindo-Zaldívar, J., Tello, A., Marín-Lechado, C., Intramontane basin development related to contractional and extensional structure interaction at the termination of a major sinistral fault: the Húercal-Overa Basin (Eastern Betic Cordillera), *Journal of Geodynamics* (2008), doi:10.1016/j.jog.2010.01.008

Intramontane basin development related to contractional and extensional structure interaction at the termination of a major sinistral fault: the Húercal-Overa Basin (Eastern Betic Cordillera)

Antonio Pedrera [(1)], Jesús Galindo-Zaldívar [(2)(3)], Alejandro Tello[(2)], and Carlos Marín-Lechado[(1)]

[1] *Instituto Geológico y Minero de España. C/ Alcázar del Genil, 4. 18006 Granada, Spain. E-mail: a.pedrera@igme.es; c.marin@igme.es*

[2] *Departamento de Geodinámica, Universidad de Granada, 18071; Granada, Spain. E-mail: jgalindo@ugr.es*

[3] *Instituto Andaluz de Ciencias de la Tierra, (CSIC-Univ. Granada), Facultad de Ciencias, Univ. Granada, 18071; Granada, Spain.*

Abstract

Among the classical minor structural associations on the termination of transcurrent faults are horsetail splays formed by reverse, normal or strike-slip faults developing duplexes. Meanwhile, temporal and spatial coexistence of contractional and extensional structures is very rarely documented. We discuss the relationships of contractional and extensional structures and associated sedimentary depocenters at the termination of a major strike-slip fault in the Eastern Betic Cordillera. Field mapping, kinematic fault analysis, paleostress determination and gravity prospecting in the Huercal Overa Basin, at the southern termination of the NE-SW Alhama de Murcia transcurrent fault (AMF), are used to establish the relationships of tectonic structures and associated sedimentary depocenters. Here, ENE-WSW and WNW-ESE folds interact with two sets of normal faults having the same orientation as well as ENE-WSW reverse faults. Progressive unconformities associated with folds reveal that the beginning of the AMF activity occurred in the Tortonian. The folds progressively grew and rotated from ENE-WSW up to WNW-ESE close to the

transcurrent fault. We propose that the development of the normal faults developed during short-term episodes characterized by vertical major stress axis and are, in turn, related to gravitational instability linked to the thickening of a crust relatively hot at depth. This setting may have become predominant in between the main activity, compressive pulses along transcurrent faults.

Keywords: Transcurrent fault, neotectonics, active tectonics, paleostress, gravity prospecting.

1. Introduction

Intramontane basin development is commonly related to extension of a previously thickened continental lithosphere. The activity of normal faults during the late evolution of the orogens results in subsidence and sedimentation. However, orogens subjected to active horizontal shortening also accommodate sediments: at the front of active thrust systems (e.g. as fore-deep basins, Beaumont, 1981; Jordan and Allmendinger, 1986; Lucente, 2004), on the top of active thrust sheets (piggy-back basins; Ori and Friend, 1984; Zoetemeijer et al., 1993), or related to strike-slip faulting (pull-apart basins; Reading, 1980; Gürbüz and Gürer 2009). The coetaneous formation of compressive and extensional tectonic structures has been addressed in some compressional settings (Burchfiel and Royden, 1985; Oldow et al., 1993; Doglioni, 1995; Decker and Peresson, 1996; Shanker et al., 2002). In these tectonic scenarios, the relation between sedimentation and tectonic structures can be complex with areas dominated by compression, sectors subjected to extension and regions with overprinted deformation. The geometry of the resulting intramontane sedimentary basins becomes irregular and numerous tectonic mechanisms have been proposed to explain their development and paleogeographic evolution.

The Neogene evolution of the Betic Cordillera (Fig. 1) is characterized by an atypical tectonic setting where both contractional and extensional structures deform the hinterland of the cordillera inducing uplift and intramontane sedimentation at least since the Tortonian (Galindo-Zaldívar et al. 2003). This setting has been traditionally explained in terms of superposition of different regional stress fields (Montenat and Ott d'Estevou 1999). These tectonic structures have a heterogeneous distribution, dominated by folds and normal faults in the central cordillera and by strike-slip faults in the eastern sector of the cordillera.

The aim of this contribution is to shed light on the relationships between the great varieties of compressive and extensional tectonic structures in order to elucidate the intramontane basin development. This research looks into the interaction of minor structures that deform the Huercal-Overa Basin, located at the southern termination of the sinistral strike-slip Alhama de Murcia Fault (Eastern Betic Cordillera). The primary objective is to discuss the relationships between compressive and extensional deformations in strike-slip fault terminations. Tectonic observations, including mapping and kinematic analysis, are combined with new gravity data to determine the sedimentary thickness distribution in order to constrain the basin development.

2. Geological setting

The Betic Cordillera (Fig. 1) has been traditionally divided into an external fold-and-thrust belt, deformed by thin-skinned tectonics and commonly referred to as the External Zones, and a mostly metamorphic hinterland called the Internal Zones. The External Zones are formed by Mesozoic and Tertiary rocks that were deposited over the

Variscan basement of the Iberian Massif, paleogeographically interpreted as a passive continental margin.

The Internal Zones are mainly formed by three major metamorphic complexes that, from bottom to top, are the Nevado-Filábride (Egeler, 1963), Alpujárride (Van Bemmelen, 1927) and Maláguide (Blumenthal, 1927). These complexes are separated by low-angle normal faults (Aldaya et al., 1984, García-Dueñas et al., 1988; Galindo-Zaldívar et al., 1989; Platt and Vissers 1989). Both the Nevado-Filábride and the Alpujárride Complexes include several thrust sheets with Paleozoic to Mesozoic lithostratigraphic sequences showing Alpine ductile deformation and metamorphism, in some cases also of Variscan age. The Maláguide Complex is formed by Paleozoic to Middle Miocene rocks that were deformed but not metamorphosed during the Alpine orogeny. The Dorsal and Predorsal complexes also belong to the Internal Zones, and are formed by Triassic to Early Neogene sedimentary rocks.

Plate-kinematic reconstructions reveal that the main deformation-driving mechanism since the middle Miocene is N-S to NW-SE shortening between Europe and Africa (e.g. Dewey et al., 1989; DeMets et al., 1994; Rosenbaum et al., 2002). Anticlockwise rotation from N-S to NW-SE occurred around 10 Ma (Rosenbaum et al., 2002). This convergence generated the relief of the Betic Cordillera, characterized by mountain ranges and depressed areas featuring sedimentary basins, respectively coinciding with large E-W to ENE-WSW antiforms and synforms. These large folds mainly interact with normal, strike-slip, and reverse faults (e.g. Booth-Rea et al., 2003). The compressive and extensional tectonic structures show features indicating simultaneous development since the Tortonian (Galindo-Zaldívar et al., 2003). The Alhama de Murcia Fault and its termination in the Huercal-Overa Basin constitute two major structures of this region.

99

100 ***2.1. The Alhama de Murcia sinistral fault (AMF)***

101 The presence of NNE-SSW to NE-SW large sinistral strike-slip faults determines
102 the neotectonic setting in Eastern Betic Cordillera (Fig. 1). This set of faults has been
103 interpreted as a large shear zone (Trans-Alborán transcurrent zone, de Larouzière et al.,
104 1988) that represents a crustal discontinuity extending southwestward, crossing the Alborán
105 Sea.

106 The Alhama de Murcia Fault (AMF) (Bousquet and Montenat, 1974) is the northern
107 segment of these transcurrent faults in the Betic Cordillera (Fig. 1). It has a NE–SW
108 orientation showing predominantly reverse strike-slip kinematics (Martínez-Díaz, 2002).
109 The AMF extends over 80 km, from Murcia as far as the Huércal-Overa Basin to the south,
110 crossing the northwest boundary of the Guadalentín depression. The most recent fault
111 activity is inferred from Quaternary sediment deformations and their geomorphological
112 expression. The AMF develops mountain fronts related to the sinistral fault segments and
113 associated folds and reverse faults (Martínez-Díaz, 2002), involving vertical axis rotation,
114 as deduced from paleomagnetic results (Mora, 1993; Krijgsman and Garcés, 2004; Mattei
115 et al., 2006). In addition, the AMF has associated low to moderate seismicity (Silva et al.,
116 1997; Stich et al., 2003, 2007).

117 Despite the numerous structural data obtained from the AMF and its surrounding
118 sedimentary basins, some questions remain open. The initial activity of AMF is under
119 debate; and while some authors propose sinistral behavior since the Tortonian (Ott
120 d'Estevou and Montenat, 1985; Montenat et al., 1987, 1990; Krijgsman et al., 2000; Vennin
121 et al., 2004) other researchers support a latest Miocene-Early Pliocene onset of activity
122 (Armijo, 1977; Meijninger and Vissers, 2006). Likewise, there is no consensus with regard

123 to the spatial and temporal distribution of stress fields proposed for this sector of the
124 cordillera from the Serravallian (Fig. 2). Bousquet and Phillip (1976b) point to E-W
125 extension from the Tortonian up to the Pliocene, plus late regional stress fields
126 characterized by horizontal N-S compression. Armijo (1977) studied the Lorca-Totana
127 sector that is located northward of the Huércal-Overa Basin, describing an extension up to
128 the Messinian and a stress field inversion characterized by compression changing from NE–
129 SW to NNE–SSW strike during the Late Pliocene, and NNW–SSE orientation during the
130 Quaternary. Other authors propose a compressive setting since the Tortonian, with
131 horizontal compression varying from NNW–SSE to NNE–SSW (Ott d'Estevou and
132 Montenat, 1985; Montenat et al., 1987, 1990; Montenat and Ott d'Estevou, 1999). Recent
133 research evidences the coexistence of NNE–SSW and NNW–SSE horizontal compression
134 and NNW-SSE horizontal extension, active during the Late Miocene to the Quaternary
135 (Martínez-Díaz, 1998, 2002). Booth-Rea et al. (2002) described extensional structures with
136 a top-to-the-W-SW transport affecting Late Serravallian age marine sediments, and sealed
137 by Lower Tortonian conglomerates in the southeastern border of the Sierra de la Tercia fold
138 (Fig. 1). These extensional structures are deformed by the Sierra de la Tercia anticline,
139 which shows an intra-Tortonian angular unconformity related to its growth. In the Bajo
140 Segura Basin, which constituted the northern termination of the AMF, Alfaro et al. (2002b)
141 describe progressive unconformities related to fold development from the Late Miocene up
142 to the present, highlighted by seismic reflection profiles. Recently, Meijninger (2006) and
143 Meijninger and Vissers (2006) put forth an inversion tectonic model where the NNE-SSW
144 to NE-SW extension was responsible for the Tortonian basin development, with inversion
145 occurring in post-Messinian times.
146

147 ***2.2. The Huércal-Overa Basin***

148 ***2.2.1. Previous models for basin development***

149 The Huércal-Overa Basin in the Eastern Betic Cordillera started to develop in the
150 Serravallian-Early Tortonian. The first studies considered it to be a pull-apart basin related
151 to strike-slip activity on NE-SW trending faults (e.g. Bousquet and Montenat, 1974).
152 Poisson et al. (1999) proposed a model where the surrounding ranges are interpreted as
153 westward-verging antiforms developed over deep-seated thrust faults, and the Huércal-
154 Overa Basin constitutes a lateral synform oriented parallel to this supposed thrust transport
155 direction. The most recent interpretations suggest the development of the Huércal-Overa
156 Basin in a purely extensional framework that favours the simultaneous exhumation and
157 thinning of the metamorphic middle to upper crust during the Late Miocene (eg. Mora,
158 1993 ; Vissers et al., 1995; Augier et al., 2004, 2005; Meijninger, 2006; Meijninger and
159 Vissers, 2006). These authors explain the compressive structures as the consequence of a
160 tectonic inversion since Late Messinian-Pliocene times.

161

162 ***2.2.2. Stratigraphy***

163 The Huércal-Overa Basin infill extends from the Middle Miocene up to the
164 Quaternary, and includes several stratigraphic units separated by unconformities (Figs. 3
165 and 4). The oldest sediments that occupy the basin are continental conglomerates (lit-de-vin
166 unit, Briend, 1981, Briend et al., 1990), possibly deposited during the Middle Miocene, yet
167 poorly represented. A thick continental red conglomerate formation, which includes
168 Nevado-Filábride pebbles, was most likely deposited during the Serravallian and Early
169 Tortonian (~12 Ma exhumation age deduced from fission-track data, Johnson, 1994 and
170 1997; Johnson et al., 1997), unconformably overlying the previous unit and the basement

rocks. The paleocurrents, mainly deduced from imbricate pebbles in this continental red conglomerate formation, are predominantly towards the E and N (Montenat et al., 1990; Meijninger, 2006), which is consistent with the flow data observed in the nearby Almanzora Corridor (Pedrera et al., 2007). These continental deposits pass gradually upwards into a variously colored sequence with alternating beds of conglomerates, sands, grey silts and gypsum, assigned to a fluvial-deltaic environment. An Early Tortonian age is evoked for this unit on the basis of foraminifera sampled in the marine levels (Briend, 1981; Guerra-Merchán and Serrano, 1993; Meijninger, 2006) and micromammals from the continental strata (Guerra-Merchán et al., 2001). At the top there is an angular unconformity where, during the Late Tortonian, bioclastic reef limestones and fan delta sediments were deposited (in the southern sector of the basin), passing into yellow marls toward the center of the basin. Foraminiferal (Guerra-Merchán and Serrano, 1993; Meijninger, 2006) and nannoplankton assemblages (Martín-Pérez, 1997) dated the marls as Late Tortonian. Messinian sediments crop out only in the easternmost part of the study area, close to the village of Huércal-Overa. During the Plio-Quaternary, detrital sediments representing alluvial fan and to the river deposits were unconformably placed over the Miocene rocks.

3. Tectonic structures in the Huércal-Overa Basin

The Late Miocene sediments that fill the Huércal-Overa Basin are quite deformed by several sets of faults and folds (Fig. 4).

3.1 Faults

Faults have been previously studied in the Eastern and Southern Huércal-Overa basin: the earliest research (Groupe de Recherche Neotectonique, 1977), was followed by

195 that of Briend (1981), and further efforts (Mora 1993; Poisson et al., 1999; Augier, 2004;
196 Meijninger and Vissers, 2006). However, data on the most recent faulting in the western
197 basin sector are scarce. We present a review of the previous data, along with a careful
198 description of the structures that deform this sector.

199 The most abundant group corresponds to WNW-ESE to NW-SE normal faults that
200 show a widespread distribution in the basin (Mora, 1993; Augier, 2004; Meijninger, 2006).
201 These faults are usually located inside the basin, presenting a length shorter than 1 km, and
202 small values of normal slip, between a few centimetres and a few meters (Fig. 4). They
203 generally dip to the SW in the northern basin sector and to the NE in the southern region.
204 The presence of conjugate faults with dihedral angles from 50º to 60º is very common
205 (Figs. 4 and 5a). Kinematic analysis of these faults generally shows a pure dip-slip
206 component. However, some fault surfaces show other striae, sometimes overprinted, that
207 suggest a local NW-SE shortening. Only the southwestern basin boundary is limited by
208 normal faults, between the villages of Albánchez and Líjar. These bounding normal faults
209 commonly present planar surfaces and tilt the Early Tortonian continental red conglomerate
210 and the Late Tortonian fan delta towards the SW. Scarce syn-sedimentary features, such as
211 bed thickness variations, show evidence of fault activity during the Tortonian.

212 This set of faults changes its geometry when deforming the multilayer sequence of
213 conglomerates, sands, grey silts, and gypsum of Early Tortonian age (Fig. 5). Flat-and-
214 ramp normal faults affect this sedimentary sequence, where the soft sedimentary layers
215 mostly concentrate the deformation and constitute detachment levels parallel to the
216 bedding. The sediments are folded by fault activity, forming roll-overs, both in the hanging
217 wall and locally in the footwall (Figs. 4 and 5). The most impressive roll-over example is
218 located close to the village of Santopetar, in the north of the study area. This structure is

219 interpreted as the result of Early Tortonian syn-sedimentary deformation in both the
220 footwall and hanging wall, along a major normal fault system composed of several flat and
221 more steeply dipping ramps (Briend, 1981; Jabaloy et al. 1993; Mora, 1993; Augier, 2004;
222 Meijninger, 2006).

223 Our field data show the presence of a second set of scarce ENE-WSW to NE-SW
224 oriented normal faults in the central part of the western Huércal-Overa Basin, deforming
225 Late Tortonian marls (Fig. 4, stations 6 and 7). The southeastern margin of the Huércal-
226 Overa basin is bounded by sub-vertical to NW-ward dipping faults of the same orientation
227 and predominantly sinistral strike-slip kinematics. However, in some fault segments normal
228 striations were observed (Fig. 4). These faults were previously interpreted as transfer fault
229 zones that accommodate the extension produced by the WNW-ESE oriented normal faults
230 (Mora 1993; Poisson et al., 1999), or else considered ancient faults active only during the
231 first stage of the basin evolution and later reactivated as sinistral faults (Augier, 2004).
232 Meijninger (2006) describes a complex history of overprinted slips in one of these faults
233 located close to Huércal-Overa village (Fig. 4), where initial dextral strike-slip striations are
234 originally overprinted by dip-slip, again overprinted by sinistral strike-slip.

235 E-W to ESE-WNW oriented subvertical dextral strike-slip faults deform the
236 Tortonian sediments that crop out mainly in the southwestern basin border close to Albox
237 (Fig. 4). These faults deform the Late Tortonian sediments and are usually sealed by the
238 Quaternary deposits (Fig. 5). However, they affect even the Quaternary deposits in the
239 central sector (Rambla el Romeral, Fig. 4). These faults may be conjugate with the NNE-
240 SSW to NE-SW large sinistral-strike-slip faults described above.

241 The Huércal-Overa Basin is deformed by reverse E-W to ENE-WSW oriented faults
242 with related folds (Fig. 6) that deform the Tortonian and, locally, the Quaternary sediments

(Groupe de Recherche Néotectonique, 1977; Briend, 1981; García Meléndez, 2000; Masana et al., 2005). In the eastern and northeastern sector of the basin, these faults form a splay geometry connected with the AMF (Briend, 1981; Silva, 1994). The Late Pliocene-Early Pleistocene faulting activity was established by the interaction of the Alhama de Murcia fault with these E–W reverse faults, generating a progressive syn-tectonic unconformity in the Garita del Diablo sector (Fig. 4) (García-Melendez et al., 2003). In the western sector of the basin, the same reverse fault set deforms the Tortonian and locally the Quaternary sediments, sometimes developing syn-tectonic growth strata during the Middle Pleistocene (Pedrera et al., 2009a and 2009c).

3.2 Folds

Most of the mountain ranges located in the Central and Eastern sectors of the Betic Cordillera correspond to km-scale antiforms, and the surrounding basins to synforms (Marín-Lechado et al., 2006 and references therein). The basin synforms developed coevally with the basin infill. Therefore, the folding age can be deduced from the progressive unconformities of the sedimentary units located near the basin boundaries. The large folds located in the study area are: the Sierra de Los Filabres and Sierra de Almagro antiforms, the Almanzora synform, and the Sierra de Las Estancias antiform (Figs. 1 and 4).

The E-W Sierra de Los Filabres antiform growth probably started during Serravallian to Early Tortonian times, as confirmed by the Serravallian-Tortonian age of the folded sediments forming progressive unconformities in the red conglomerate unit, and also in the overlying Late Tortonian sediments (Pedrera et al., 2007). The northward and eastward flow directions deduced in the red conglomerate formation during the Serravallian-Early Tortonian (Montenat et al., 1990; Meijninger, 2006) points to an

267 enhanced topography in the Sierra de Los Filabres, where there was erosion and an
268 abundant sediment supply. The Sierra de Las Estancias does not act as a barrier to sediment
269 transport. In fact, uplift of the Sierra de Las Estancias started later, during the Tortonian
270 (Pedrera et al., 2007).

271 The Almanzora Corridor is determined by an N-vergent large synform with
272 direction changing from E-W near the western corridor to ENE-WSW at the eastern end,
273 near the Huércal-Overa Basin. This synform deforms all the Miocene sediments and
274 determines the location of the pelagic sediments in its core. The Quaternary continental
275 alluvial fan beds have initial sedimentary dips towards the centre of the basin, and they lie
276 unconformably over the folded marine sediments, precluding to determine if they are
277 folded.

278 The Sierra Almagro, located in the Eastern prolongation of the Sierra de Los
279 Filabres (Figs. 1 and 4), is also an ENE-WSW oriented antiform that deforms the Tortonian
280 and Messinian sediments. Its limbs are strongly affected by faults, and ENE-WSW oriented
281 North-western dipping reverse faults control its southern mountain front (Rutter et al.,
282 1986; Booth-Rea et al., 2004). The northern limb is deformed by the sub-vertical ENE-
283 WSW to NE-SW oriented faults described above, as they constitute the boundary of the
284 Huércal-Overa basin.

285 In addition to these large folds, the Huércal-Overa Basin sediment is deformed by
286 minor folds (Figs. 4 and 6). They could be grouped, according to the mean strike, as ENE-
287 WSW or WNW-ESE oriented folds. Both sets of folds have wavelengths of tens to
288 hundreds of meters, being generally open folds, although they occasionally show vertical
289 limbs. Their vergence is variable: for example, in the centre of the basin the antiforms are
290 usually S-vergent with a northern limb characterized by gentle dip to the North and a

steeply dipping to vertical southern limb (e.g. La Parata sector). On the other hand, the folds in the Western sector are usually N-vergent (e.g. La Molata fold, Pedrera et al., 2009a).

In the central sector of the Basin, the sediments and the metamorphic rocks of Sierra Limaria (Fig. 4) are deformed by a band of WNW-ESE oriented open folds. The fold wavelengths vary between 1 and 4 km, and their strike is up to 30º oblique to the main normal fault set. There is no a consensus in the interpretation of these folds. While some authors associate them with compression or transpression (Poisson et al., 1999), others interpret them as extensional roll-over anticlines developed above listric normal faults (Meijninger, 2006). In some places the normal faults are tilted, and in some outcrops the normal faults deform the tilted strata (Fig. 5). In the Huércal-Overa Basin, the roll-overs are usually related to listric or flat-and-ramp normal faults that deform the multi-layered sequence of conglomerates, sands, grey silts and gypsum, or the sediments placed immediately atop this unit (Fig. 5).

4. Paleostress results

In order to complete the previous paleostress studies in the Huércal-Overa Basin (Mora, 1993; Augier, 2004; Meijninger and Vissers, 2006), stress inversion of the measured faults located in the western sector of the basin was performed following the Galindo-Zaldívar and González-Lodeiro (1988) method. This method uses a systematic search on a grid pattern and allows determining overprinted stress ellipsoids including main axes orientations and axial ratios. The calculated stress ellipsoids (Fig. 7 and Table 1) could be grouped into three different main sets. (a) The best represented group (type 1) is characterized by a sub-vertical maximum stress axis, NNE-SSW to NE-SW sub-horizontal

extension, and variable axial ratios that are in transition to prolate ellipsoids of radial extension. This group is related to normal faults that are WNW-ESE and NW-SE oriented (stations: 1, 2, 3, 4, 5, 8 phase I, 17, 18 and 19, 20, 24, 25, 26, 27 and 28). The maximun axis observed in some stations plunges, suggesting the rotation of the faults by late folds (Table 1, stations 22 and 23). (b) The second set (type 2) has a sub-vertical maximum stress axis, E-W to NW-SE extension and low axial ratios, also related to prolate ellipsoids of radial extension (stations: 6, 7, 8 phase II and 29). (c) The third group pertains to stress ellipsoids with a NW-SE sub-horizontal maximum stress axis and low-to-medium axial ratios, likewise suggesting prolate to intermediate ellipsoids related to the development of compressive structures like ENE-WSW reverse faults and folds (9, 10 and 14 phase I).

5. Gravity survey

In contrast to the widespread geological studies developed in the area (Meijninger and Vissers, 2006, and references therein), there are practically no detailed geophysical studies in the sector that help to constraint the thickness of the sedimentary rocks. Vertical electric sounding data alone allowed García-Meléndez et al. (2003) an approximate reconstruction of the three-dimensional shape of the Cubeta del Saltador, located in the northeastern Huércal-Overa Basin (Fig. 4). For this reason, new gravity data were acquired and interpreted in the light of the available geological information in order to determine the deep structure of the Huércal-Overa Basin.

5.1. Gravity data acquisition and processing

Gravity data were acquired by means of a Scintrex cg-5 gravity-meter, with a maximum accuracy of 0.001 mGal. The relative positioning of the gravity stations was

done with a e-trex Garmin GPS receiver, and the heights of the stations were determined with a barometric altimeter with an accuracy of 0.5 m. Gravity measurement stations are located along four profiles that are approximately NNW-SSE orientated (Fig. 4). These profiles constitute complete sections of the basin, from the Sierra Almagro-Sierra de Los Filabres up to Sierra de Las Estancias, crossing through the Sierra Limaria. The average distance between stations along the profiles was 250 m.

The gravity measurements were established with reference to the Baza gravimetric base (-2º 46' 41.9", 37º 29' 12.0"; *Instituto Geográfico Nacional, www.ign.es*), which allows us to determine the absolute gravity values along the profiles. After tidal and instrumental drift, the Bouguer anomaly was obtained using a reference density of 2.67 g/cm^3 and applying the topographic correction to a radius of 22 km, calculated from a digital elevation model with a grid of 90 m, following the Hammer method (Hammer, 1939, 1982). The influence of topography outside of this 22 km radius tends to smoothly affect the Bouguer anomaly, and was corrected with the regional anomaly subtraction during the residual anomaly determination. The residual gravity anomaly map (Fig. 8) was calculated from the Bouguer anomaly by profile interpolation, and subtracting the regional anomaly determined on the basis of 46 measurements over basement rocks in agreement with the regional anomaly maps (IGN, 1975). Finally, residual 2D gravity models along the measured profiles were developed with GRAVMAG v. 1.7 software (Pedley et al. 1993).

5.2. Gravity modelling and deep structure

The new gravity data allow us to illustrate the sedimentary infill thickness (Figs. 8 and 9) with a complex pattern where the minimum values (-12 mGal) are reached in the central part of the western Huércal-Overa Basin. Residual gravity anomalies were

363 considered together with surface observations in order to determine the deep structure of
364 the basin by 2D modelling (Fig. 9). For gravity modelling, an average density of 2.35 g/cm^3
365 was considered for the whole sedimentary infill (Robinson and Çoruh 1988; Telford et al.
366 1990), also in agreement with gravity studies previously developed in other sedimentary
367 basins of the Betic Cordillera, with similar lithostratigraphic sequences (Marín-Lechado et
368 al., 2006; Pedrera et al., 2006 and 2009b). However, to evaluate the uncertainty in the basin
369 infill thickness determination we present alternative gravity models assuming the minimum
370 and the maximum plausible density contrasts (2.2-2.5 g/cm^3 sediments, 2.67 g/cm^3
371 basement). The obtained gravity anomalies for each profile are irregular in shape, with
372 minimum values between -12 mGal and -2.5 mGal. The sedimentary infill distribution
373 obtained from the models is also irregular, reaching up to 1000 meters of maximum
374 thickness in profile 2 (using the middle density contrast).

375 The combination of the 2D gravity models and the geological field observations
376 allows us to associate the sediment distribution with the tectonic structures and constrain
377 the geological cross-sections (Fig. 10). The residual anomaly map and the 2D model of
378 profile 2 show the maximum sedimentary thickness to coincide with the ENE-WSW
379 Almanzora synform hinge. Other minor discontinuities could be related to normal faults.
380 However, the faults bounding the southern sector of the basin have no associated important
381 thickness of sediments, as might be initially expected.

382

383 **6. Discussion**

384 The interaction of compressional and extensional structures is recorded by the
385 sedimentary infill of the Huércal-Overa Basin. This tectonic framework could be partially a
386 consequence of the southern termination of the Alhama de Murcia transcurrent fault. In this

setting, we first present a discussion of the age of basin development and fault activity so as to highlight their relationships. The main geometric features of the sedimentary basin are then constrained to constitute new data for discussion of previously proposed regional models. This discussion is focused on the coexistence of extensional and compressional deformations responsible for the geological evolution of the region since Tortonian.

6.1 Onset and evolution of the Alhama de Murcia Fault deduced from fold growth

In contrast to reverse and normal faults, which usually have associated wedge deposits that record their progressive development, it is quite difficult to date the initial activity of a strike-slip fault. Notwithstanding, one can identify the first occurrence of strike-slip faulting by studying the associated folds, and normal and/or reverse faults.

Local contractional minor structures related to the AMF hold the key to establishing their complete history. The AMF presents a complete set of related folds and reverse faults in its central sector (Sierra de la Tercia fold, Booth-Rea et al., 2002, and Martínez Díaz, 2002), and located at its terminations (to the North in the Bajo Segura Basin splay and related folds: Silva, 1994, Alfaro et al., 2002a and 2002b; and to the South in the Huércal-Overa Basin: García-Meléndez et al., 2003). By the northern termination of the AMF, seismic profiles point to the existence of progressive unconformities related to ENE-WSW folds (Alfaro et al., 2002b). In the central sector, Booth-Rea et al. (2002), from field observations, described Tortonian tilted sedimentation related to the Sierra de la Tercia antiform uplift. In the southern termination of the AMF, our structural data point to the presence of a WNW-ESE minor fold band that was active during the Tortonian, before the deposition of Late Tortonian sediments, as deduced from the progressive unconformities associated with the fold limbs. The activity of the AMF continued during the Plio-

411 Pleistocene, as could be deduced from the syn-tectonic progressive unconformity located in
412 the Garita del Diablo sector (García-Melendez et al., 2003), and during the Holocene
413 (Masana et al., 2005). Thus, field observations support the hypothesis of the Late Tortonian
414 to present-day activity of the AMF.
415
416 ***6.2 Basin development models***
417 The most recent models proposed for the Huércal-Overa basin by Meijninger (2006)
418 and Meijninger and Vissers (2006) conclude that it is an extensional basin developed on an
419 extending underlying crust and lithosphere since the Middle Miocene. In addition, these
420 authors propose that some parts of the Alhama de Murcia fault zone initiated as normal
421 faults, which were later reactivated as strike-slip-reverse faults. Our results are in
422 agreement with the development of normal faults that mainly accommodate ENE-WSW to
423 NE-SW extension during the Tortonian. However, geological cross-sections constructed
424 from field data and gravity models indicate that there is no great depocenter linked to the
425 southern border faults (Fig. 10).
426 The Huércal-Overa Basin has to be explained in the framework of the AMF activity
427 together with the large folds and normal faults formed since the Tortonian. Although
428 sedimentary basins commonly form by the extension of the crust, often they develop in
429 sectors subjected to horizontal shortening, where folding significantly influences their
430 location, dimension, and geometry (Cobbold et al., 1993; Nicol et al., 1994). In
431 contractional tectonic settings other authors have described the coetaneous formation of
432 compressive and extensional structures, e.g. in the Himalaya (Burchfiel and Royden, 1985;
433 Shanker et al., 2002), and in several sectors of the Mediterranean region along the Alpine
434 mountain range (Oldow et al., 1993; Decker and Peresson, 1996). The geometry of these

435 sedimentary basins became irregular, and the relationship between their sedimentation and
436 tectonic structures could be complex, featuring sectors dominated by compression or by
437 extension, or sectors with overprinted deformation.

438 Our structural data prove active NW-SE compression since the Tortonian, causing
439 the development of folds and faults. Progressive unconformities, associated with large and
440 minor folds, evidence continuous deformation. In addition, the maximum sedimentary
441 thickness is related to the eastward continuation of the Almanzora synform (Fig. 10), which
442 represents one of the main compressive structures of the region. The E-W to ENE-WSW
443 synform development favoured a transgression during the Late Tortonian (Pedrera et al.,
444 2007). Despite the presence of numerous normal faults, the existence of a succession of
445 antiforms and synforms along fold bands also suggests a compressive origin. In a purely
446 extensional framework, only single and isolated roll-overs occur.

447 At any rate, WNW-ESE to NW-SE oriented normal faults were active since the
448 Early Tortonian, also indicating the presence of extensional stress ellipsoids —type 1— in
449 the whole basin. Moreover, normal faults that developed in an extensional setting with type
450 2 ellipsoids, are parallel to the ENE-WSW folds, probably corresponding to external arc
451 extensions, and deform the Tortonian marls close to the Almanzora synform hinge.

452 In addition, minor folds and reverse faults that are ENE-WSW oriented began to
453 grow probably in the Late Tortonian, favouring basin emersion and erosion. In the western
454 sector of the basin, these structures accommodate NW-SE shortening, related to stress
455 fields represented by type 3 ellipsoids.

456

457 ***6.3 Compressive and extensional tectonic structures in a strike-slip fault termination***

458 Associations of compressive and extensional minor structures linked to
459 transcurrence have been widely recognized in the field (Freund, 1974; Woodcock and
460 Fisher, 1986), and their mechanisms of development have been tested through analogue
461 models (Tchalenko 1970, Hempton and Neher, 1986; Naylor et al., 1986). The classical
462 minor structural associations on the transcurrent fault termination are sets of splay faults,
463 either normal or reverse. The new structural data reported in this paper promote the
464 discussion of compressive and extensional tectonic structural interaction in a strike-slip
465 fault termination.

466 In the surroundings of the Alhama the Murcia sinistral strike-slip Fault, the presence
467 of normal faults and compressive tectonic structures has most often been explained by
468 successive stress field changes since the Serravallian (Bousquet and Phillip, 1976a, 1976b;
469 Armijo, 1977; Montenat et al., 1987, 1990; Ott d'Estevou and Montenat, 1985 and 1999;
470 Augier, 2004; Meijninger, 2006; Meijninger and Vissers, 2006). Recently, models have
471 proposed attempting to compile the array of tectonic structures under a regional stable
472 stress field (Martinez-Díaz et al., 2002; Pedrera et al., 2007), according to the NW-SE
473 regional shortening direction obtained from the plate-kinematic reconstruction models
474 (Dewey, 1989; Srivastava et al., 1990; Muller and Roest, 1992; Mazzoli and Helman, 1994;
475 Rosenbaum et al., 2002).

476 In the framework of the regional NW-SE Eurasian-African plate convergence (De
477 Mets, 1994), the new data presented suggest a coeval development since the beginning of
478 the Tortonian of compressive and extensional structures under the same regional stress
479 field. The folds are related to regional compression (ENE-WSW oriented folds) as well as
480 to the strike-slip fault termination (both WNW-ESE and ENE-WSW oriented folds). While
481 the ENE-WSW folds deform up to the Quaternary sediments, the WNW-ESE folds only

deform Tortonian sediments. We propose that AMF activity produce the clockwise vertical axis rotation of the folds at its ends, the initially ENE-WSW folds thereby become WNW-ESE oriented and inactive (Fig. 11A and B). These changes in fold orientation are also supported by palaeomagnetic data (Mora, 2003; Mattei et al., 2006). Afterwards, the activity of the transcurrent fault was accommodated by new ENE-WSW oriented folds and reverse faults forming a common splay geometry that interacts with all the previous structures (Fig. 11 D).

We propose two possible mechanisms to support the development of normal faults with the same orientations as folds (Fig. 11 C). (a) The first possibility is a decrease in the horizontal compressive stress produced by relaxation after major transcurrent activity pulses of the AMF. In regions subjected to crustal shortening, transcurrent faults generally show highly variable spatial and temporal slip rates (Benett et al., 2004; Chevalier et al., 2005). When the horizontal stress diminishes, normal faults may start to develop because the vertical stress axis reaches a maximum induced by gravity. (b) The second hypothesis that may explain the normal fault development is related to the progressive thickening of the crust, which was relatively hot at depth. The available geophysical data (Banda and Ansorge, 1980; Banda et al., 1993; Pous et al., 1999) and the most recent thermal model (Soto et al., 2008) suggest a crust relatively hot in its deepest part decoupled from an anomalous mantle in the Eastern Betic Cordillera. A general uplift, together with emersion and erosion of the Late Miocene basins, is well documented since the Early Tortonian (Braga et al., 2003). In addition, crustal anatexix processes occurring at depth between 12 and 9 Ma, as have been deduced from the mineral age of enclaves located in the high-calalkaline volcanic rocks cropping out in the Eastern Betics (Álvarez-Valero and Kriegsma, 2007; Cesare et al., 2008). In addition, the extrusion of calc-alkaline and

506 tholeitic volcanic rocks extend from Tortotian up to Messinian in the Eastern Betic, Rif
507 cordilleras and in the Alborán Sea (Duggen et al., 2008 and reference therein). Alkali
508 basalts extruded in Mazarrón-Cartagena area during the Pliocene, as occur in other zones of
509 the Rif Mountains (Duggen et al., 2008). An isostatic response linked to progressive crustal
510 thickening and the partial melting of the deepest crust would have resulted in a potential-
511 energy increase and instability in the upper crust, producing normal faulting. Both
512 mechanisms could work together and explain the presence of the sub-vertical maximum
513 stress axis and sub-horizontal extension, NNE-SSW to NE-SW and E-W to NW-SE, in
514 transition to radial extension.
515
516 **7. Conclusions**
517 Compressive and extensional structures deformed the Late Miocene-Quaternary
518 Huércal-Overa Basin, located in the southern termination of the Alhama de Murcia sinistral
519 fault (AMF). Progressive unconformities associated with the fold limbs reveal a Tortonian
520 onset of its activity. Analysis of fold and fault development, gravity data, and the
521 paleostress inversion from minor structures altogether reveal the coeval interaction of three
522 main stress fields (ellipsoids 1 to 3) in a setting of regional NW-SE plate convergence and
523 crustal thickening since the Tortonian.
524 The compressive structures comprise the major NE-SW to NNE-SSW Alhama de
525 Murcia sinistral fault, kilometric folds and small scale ENE-WSW reverse faults and folds
526 that are developed by a NW-SE oriented sub-horizontal maximum stress axis (ellipsoid 3).
527 In this setting, the eastward extension of the large Almanzora synform constitutes the main
528 structure determining the Huercal-Overa depocenter. Minor folds progressively grew and

529 rotated from ENE-WSW up to WNW-ESE, becoming inactive with the clockwise vertical
530 axis rotation close to the transcurrent fault termination.

531 Meanwhile, a sub-vertical maximum stress axis and sub-horizontal extension NNE-
532 SSW to NE-SW (ellipsoids 1) and E-W to NW-SE oriented, in transition to radial extension
533 (ellipsoids 2) is responsible for the widespread normal fault development. This stress
534 setting could be explained as a consequence of potential-energy increase related to the
535 thickening of a crust relatively hot at depth, or/and by a decrease in the horizontal stress
536 between activity pulses of the Alhama de Murcia fault. Both mechanisms serve to explain a
537 temporary major vertical stress axis induced by gravity.

538 The field example tackled in this contribution illustrates the coalescence of
539 compressional and extensional structures interacting in the termination of a large
540 transcurrent fault. The proposed genetic models reconcile the great amount of apparently
541 incompatible previous data with new geological and geophysical observations.

542

543 **Acknowledgements**

544 We are grateful Reinoud Vissers, John Platt, Jan-Philipp Schmoldt, and an
545 anonymous reviewer the comments and suggestion on an early version of the paper. This
546 study was supported by the projects TOPO-IBERIA CONSOLIDER-INGENIO CSD2006-
547 00041 and CGL 2006-06001 of the Spanish Ministry of Science and Education, as well as
548 by Research Group RNM-149 of the Junta de Andalucía Regional Government. Jean
549 Sanders revised the English manuscript style.

550

551 **References**

552

553 Aldaya, F., Campos, J., García-Dueñas, V., González-Lodeiro, F., Orozco, M. (1984). El contacto
554 Alpujárrides/Nevado-Filábrides en la vertiente meridional de Sierra Nevada. Implicaciones
555 tectónicas. In: El borde mediterráneo español: evolución del orógeno bético y geodinámica
556 de las depresiones neógenas. Departamento de Investigaciones Geológicas, C.S.I.C. and
557 Universidad de Granada, Granada, ISBN 00-05776-7, 18–20.

558 Alfaro, P., Andreu, J. M., Delgado, J. Estévez , A. Soria, J. M., Teixido, T. (2002a). Quaternary
559 deformation of the Bajo Segura blind fault (eastern Betic Cordillera, Spain) revealed by
560 high-resolution reflection profiling. Geological Magazine, 139, 331-341. doi:
561 10.1017/S0016756802006568

562 Alfaro P., Delgado, J., Estévez, A., Soria, J.M., Yébenes, A. (2002b). Onshore and offshore
563 contractional tectonics in the eastern Betic Cordillera (SE Spain). Marine Geology, 186,
564 337-349.

565 Álvarez-Valero, A. M. and Kriegsman, L. M. (2007). Crustal thinning and mafic underplating
566 beneath the Neogene Volcanic Province Betic Cordillera, SE Spain , evidence from crustal
567 xenoliths, Terra Nova, 19 4 , 266, doi,10.1111/j.1365-3121.2007.00745.x.

568 Armijo, R. (1977). La zone des failles Lorca–Totana (Cordillères Bétiques, Espagne). Étude
569 tectonique et neotectonique. MsC Thesis, University, Paris VII.

570 Augier R. (2004). Evolution tardi-orogénique des Cordilères Bétiques (Espagne): Apports d'un
571 étude intégrée, Ph.D. thesis, Univ. de Pierre et Marie Curie, Paris.

572 Banda, E. and Ansorge, J. (1980). Crustal structure under the central and eastern part of the Betic
573 Cordillera. Geophys. J. Roy. Astr. Soc. 63, 515-532.

574 Banda, E., Gallart, J., García Dueñas, V., Dañobeitia, J. J., Makris, J. (1993). Lateral variation of
575 the crust in the Iberian Peninsula, new evidence from the Betic Cordillera. Tectonophysics,
576 221, 53-66.

577 Beaumont, C. (1981). Foreland basins. Geophys. J. R. Astron. Soc. 65, 291–329. Benett, R.,
578 Friedrich, A., Furlong, K. 2004. Codependent histories of the San Andreas and San Jacinto
579 fault zones from inversion of fault displacement rates. Geology, 32, 961-964.

580 Blumenthal, M. (1927). Versuch einer tektonischen Gliederung der Betischen Kordilleren von
581 Central und Sùdwest Andalusien. Eclogae Geol. Helv., 20, 487-592.

582 Booth-Rea, G., Azañón, J.M., Azor, A., García-Dueñas, V. (2004). Influence of strike-slip fault
583 segmentation on drainage evolution and topography. A case study: the Palomares Fault
584 Zone (southeastern Betics, Spain). Journal of Structural Geology 26, 1615-1632.

585 Booth-Rea, G., Azañón, J.M., García-Dueñas, V., Augier, R. (2003). Uppermost Tortonian to
586 Quaternary depocentre migration related with segmentation of the strike-slip Palomares
587 Fault Zone, Vera basin, SE Spain. Comptes Rendus Geoscience 335, 751-761.

588 Booth-Rea, G., García-Dueñas, V., Azañón J.M. (2002). Extensional attenuation of the Malaguide
589 and Alpujarride thrust sheets in a segment of the Alborán basin folded during the Tortonian
590 (Lorca area, Eastern Betics). C. R. Geoscience 334, 557-563.

591 Bousquet, J.C. and Montenat, C. (1974). Presence de décrochements NE–SW plio-quaternaires dans
592 les Cordillères Bétiques Orientales (Espagne). Extension et signification général. Comptes
593 Rendus de l'Academie des Sciences Paris 278, 2617-2620.

594 Bousquet, J.C. and Phillip, H. (1976a). Observations micro-tectoniques sur la distension plio-
595 pleistocene ancien dans l'est des Cordillères Bétiques (Espagne méridionale). Cuadernos de
596 Geología, Universidad de Granada 7, 57-67.

597 Bousquet, J.C. and Phillip, H. (1976b). Observations micro-tectoniques sur la compresion nord-sud
598 quaternaire des Cordillères Bétiques Orientales (Espagne Méridional—Arc de Gibraltar).
599 Bulletin Societé Géologique de France 18, 711-724.

600 Briend, M. (1981). Evolution morpho-tectonique du bassin néogène de Huercal-Overa (Cordillères
601 bétiques orientales, Espagne). Ph.D. Thesis, Institut Geologique Albert de Lapparent, 208
602 pp.

603 Briend, M., Montenat, C., Ott d´Estevou, P. (1990). Le bassin de Huercal-Overa. In, C. Montenat
604 Editor , Les bassins Neogenes du Domaine Betique Oriental Espagne , pp. 239-259.

605 Burchfiel, B.C. and Royden, L.H. (1985). North-south extension within the convergent Himalayan
606 region Geology 13, 10, 679-682.

607 Cesare, B., Rubatto, D., Gómez-Pugnaire, M.T. (2008). Do extrusion ages reflect magma
608 generation processes at depth? An example from the Neogene Volcanic Province of SE
609 Spain, Contrib Mineral Petrol, doi,10.1007/s00410-008-0333-x.

610 Chevalier, M.L., Ryerson, F. J., Tapponnier, P., Finkel, R. C., Van Der Woerd, J., Li Haibing, and
611 Liu Qing, (2005). Slip-Rate Measurements on the Karakorum Fault May Imply Secular
612 Variations in Fault Motion. Science, 307, 411-414.

613 Cobbold, P.R., Davy, P., Gapais, D., Rossello, E.A., Sadybakasov, E., Thomas, J.C., Tondji Biyo,
614 J.C. and De Urreiztieta, M. (1993). Sedimentary basins and crustal thickening. In: S.
615 Cloetingh, W. Sassi, F. Horvath and C. Puigdefabregas (Eds.), Basin Analysis and
616 Dynamics of Sedimentary Basin Evolution. Sediment. Geol. 86, 77-89.

617 Decker, K. and Peresson, H. (1996). Tertiary kinematics in the Alpine-Carpathian-Pannonian
618 system: links between thrusting, transform faulting and crustal extension. In: Wessely, G.,
619 Liebl, W. (Eds.), Oil and Gas in Alpidic Thrustbelts and Basins of Central and Eastern
620 Europe. EAGE Spec. Publ., 5, 69-77.

621 De Larouzière F.D., Bolze J., Bordet P., Hernández J., Montenat C., Ott d'Estevou P. (1988). The
622 Betic segment of the lithospheric Trans-Alboran shear zone during the Late Miocene.
623 *Tectonophysics* 152, 41-52.

624 DeMets, C., Gordon, R.G., Argus, D.F., Stein, S. (1994). Effect of recent revisions to the
625 geomagnetic reversal time scale on estimates of current plate motions. Geophys. Res. Lett.
626 21, 2191-2194.

627 Dewey, J.F., Helman, M.L., Turco, E., Hutton, D.H.W., Knott, S.D. (1989). Kinematics of the
628 Western Mediterranean. In: Coward, M.P., Dietrich, D., Park, R.G. (Eds.), Alpine
629 Tectonics. Special Publication Geological Society of London, 265-283.

630 Doglioni, C. (1995). Geological remarks on the relationships between extension and convergent
631 geodynamic settings. Tectonophysics 252, 253-267

632 Duggen, S., Hoernle, K., Klügel, A., Geldmacher, J., Thirlwall, M., Hauff, F., Lowry, D., Oates, N.
633 (2008). Geochemical zonation of the Miocene Alborán Basin volcanism westernmost
634 Mediterranean, geodynamic implications Contrib. Mineral Petrol. doi, 10.1007/s00410-008-
635 0302-4

636 Egeler, C. and Simon, O.J. (1969). Sur la tectonique de la Zone Bétique (Cordillères Bétiques,
637 Espagne). Verhandelingen der Koninklijke Nederlandse Akademie van Weten-schappen 25,
638 90 pp.

639 Freund, R. (1974). Kinematics of transform and transcurrent faults.Tectonophysics 21, 93-134.

640 Galindo-Zaldívar, J., Gil, A.J., Borque, M.J., González-Lodeiro, F., Jabaloy, A., Marín-Lechado, C.,
641 Ruano, P., Sanz de Galdeano, C. (2003). Active faulting in the internal zones of the central
642 Betic Cordilleras (SE Spain). J. Geodynamics 36, 239-250.

643 Galindo-Zaldívar, J. and González Lodeiro, F. (1988). Faulting phase differentiation by means of
644 computer search on a grid pattern, Annales Tectonicae 2, 90-97.

645 Galindo-Zaldívar, J., González Lodeiro, F., Jabaloy, A. (1989). Progressive extensional shear
646 structures in a detachment contact in the western Sierra Nevada (Betic Cordilleras, Spain).
647 Geodinámica Acta 3, 73-85.

García-Dueñas, V., Martínez-Martínez, J.M., Orozco, M., Soto, J. (1988). Plisnappes, cisillements syn- à post-métamorphiques et cisaillements ductilesfragiles en distension dans les Nevado-Filabrides (Cordillères bétiques, Espagne). Comptes Rendus de l'Académie des Sciences de Paris 307, 1389-1395.

García-Meléndez, E. (2000). Geomorfología y Neotectónica del Cuaternario de la cuenca de Huércal-Overa y corredor del Almanzora. Análisis y Cartografía mediante Teledetección y SIG. Ph.D. Thesis. Universidad de Salamanca.

García-Meléndez, E., Goy, J.L., Zazo, C. (2003). Neotectonics and Plio-Quaternary landscape development within the eastern Huercal-Overa Basin (Betic Cordilleras, Southeast Spain). Geomorphology 50, 111-133.

Guerra-Merchán, A., Ramallo, D., Ruiz Bustos, A. (2001). New data on the Upper Miocene micromammals of the Betic Cordillera and their interest for marine-continental correlations. Geobios 34, 85-90.

Guerra-Merchán, A. and Serrano, F. (1993). Tectonosedimentary setting and chronostratigraphy of the Neogene reefs in the Almanzora corridor (Betic Cordillera, Spain). Geobios 26 , 57-67.

Gürbüz, A. and Gürer, O. F. (2009). Middle Pleistocene extinction process of pull-apart basins along the North Anatolian Fault Zone.Physics of the Earth and Planetary Interiors, 173, 177-180

Groupe de recherche Néotectonique de l´Arc de Gibraltar. 1977. L'histoire tectonique récente (Tortonien à Quaternaire) de l'Arc de Gibraltar et des bordures de la mer d'Alboran. Bulletin de la Société géologique de France 19: 575-614.

Hammer, S. (1939). Terrain Corrections for Gravity Stations, Geophysics, 4, 184-194.

Hammer, S. (1982). Critique of Terrain Corrections for Gravity Stations, Geophysics, 47, 839-840.

671 Hempton, M.R. and Neher, K. (1986). Experimental fracture, strain and subsidence patterns over en
672 echelon strike-slip faults: implications for the structural evolution of pull-apart basins.
673 Journal of Structural Geology 8, 597-605.

674 I.G.N. (1975). Mapa de España de Anomalía de Bouguer. I.G.N., Madrid. Scale 1:1000000.

675 Jabaloy, A., Galindo-Zaldívar, J., Guerra-Merchán, A., González-Lodeiro, F. (1993). Listric normal
676 faults: constraints to the geometric and kinematic analysis from the study of natural
677 examples. Document du BRGM (Late orogenic extension in mountain belts, Montpellier,
678 France), 219, 100-101.

679 Johnson, C. (1994). Neogene tectonics in south eastern Spain: Constraints from fission track
680 analysis, Ph.D. Thesis, Univ. of London, London.

681 Johnson, C. (1997). Resolving denudational histories in orogenic belts with apatite fission-track
682 thermochronology and structural data: An example from southern Spain, Geology, 25, 623-
683 626.

684 Johnson, C., Harbury, N., Hurford A.J. (1997). The role of extension in the Miocene denudation of
685 the Nevado-Filábride Complex, Betic Cordillera (SE Spain), Tectonics, 16, 189-204.

686 Jordan, T.E., Allmendinger, R.W. (1986). The Sierras Pampeanas of Argentina: a modern analogue
687 of Rocky Mountain foreland deformation, Am. J. Sci. 286, 737-764.

688 Krijgsman, W., Garcés, M. (2004). Palaeomagnetic constraints on the geodynamic evolution of the
689 Gibraltar Arc. Terra Nova, 16, 281-287.

690 Krijgsman, W., Garcés, M., Agustí, J., Raffi, I., Taberner, C. and Zachariasse, W.J. (2000). The
691 'Tortonian salinity crisis' of the eastern Betics (Spain). Earth and Planetary Science Letters,
692 181, 497-511.

693 Lucente, C.C. (2004). Topography and palaeogeographic evolution of a middle Miocene foredeep
694 basin, northern Apennines, Italy. Sedimentary Geology 170, 107-134.

695 Marín-Lechado, C., Galindo-Zaldivar, J., Rodríguez-Fernández, L.R., Pedrera A. (2006). Mountain
696 front development by folding and crustal thickening in the Internal Zone of the Betic
697 Cordillera-Alboran Sea Boundary. Pure Appl. Geophys. 164, 1-21, doi :10.1007/s00024-
698 006-0157-4.

699 Martín-Pérez, A. (1997). Nannoplancton calcáreo del Mioceno de la Cordillera Bética (Sector
700 Oriental). Ph.D. Thesis. Universidad de Granada.

701 Martínez Díaz, J.J. (2002). Stress field variation related to fault interaction in a reverse oblique-slip
702 fault: the Alhama de Murcia fault, Betic Cordillera, Spain. Tectonophysics, 356, 291-305.

703 Martínez Díaz, J.J. (1998). Neotectónica y Tectónica Activa del sector centrooccidental de Murcia y
704 Sur de Almería, Cordillera Bética (España). Ph.D. Thesis, Universidad Complutense de
705 Madrid.

706 Masana, E, Martínez-Díaz, J.J., Hernández-Enrile, J.L., Santanach, P. (2004). The Alhama de
707 Murcia fault (SE Spain), a seismogenic fault in diffuse plate boundary. Seismotectonic
708 implications for the Ibero-Magrebian region. J. Geophys. Res. 109: 1-17.

709 Masana, E., Pallàs, R,. Perea, H., Ortuño, M., Martínez-Díaz, J.J., García-Meléndez, E., Santanach,
710 P. (2005). Large Holocene morphogenic earthquakes along the Albox fault, Betic
711 Cordillera, Spain. J. Geodynamics 40, 119-133, doi: 10.1016/j.jog.2005.07.002.

712 Mattei, M., Cifelli, F., Martín Rojas, I., Crespo Blanc, A., Comas, M., Faccenna, C., Porreca M.
713 (2006). Neogene tectonic evolution of the Gibraltar Arc: New paleomagnetic constraints
714 from the Betic chain. Earth and Planetary Science Letters 250, 522-540.

715 Mazzoli, S., Helman, M.L. (1994). Neogene patterns of relative plate motion for Africa-Europe:
716 some implications for recent central Mediterranean tectonics. Geologische Rundschau 83,
717 464-468.

718 Meijninger, B.M.L. (2006). Late-orogenic extension and strike-slip deformation in the Neogene of
719 southeastern Spain. Ph.D. Thesis, Universiteit Utrecht. Geologica Ultraiectina.

720 Meijninger, B.M.L., Vissers, R.M.L. (2006). Miocene extensional basin development in the Betic
721 Cordillera, SE Spain, revealed through analysis of the Alhama de Murcia and Crevillente
722 Faults. Basin Research 18, 547-571. doi: 10.1111/j. 1365-2117.2006.00308.x.

723 Montenat, C., Ott d'Estevou, P. (1996). Late Néogène basins evolving in the Eastern Betic
724 transcurrent fault zone: an illustrated review. In: Friend, P.F., Dabrio, C. (Eds.), Tertiary
725 Basins of Spain. Cambridge Univ. Press, Cambridge, 372-387.

726 Montenat, C., Ott d'Estevou, P., Masse, P. (1987). Tectonic–sedimentary characters of the Betic
727 Néogène Bassins evolving in a crustal transcurrent shear zone (SE Spain). Bulletin du
728 Centre de Recherches Exploration Production Elf Aquitaine 11, 1-22.

729 Montenat, C., Ott d'Estevou, Ph., Delort, T. (1990). Le Bassin de Lorca. Doc. Trav. I.G.A.L 12-13,
730 239-259.

731 Montenat, C., Ott d'Estevou, P. and Aelllen de la Chapelle, M. (1990). Les series Neogenes entre
732 Lorca et Huercal Overa. Documents et Travaux de l'Institut Geologique Albert de
733 Lapparent (IGAL), 12-13, 281-286.

734 Montenat C. and Ott d'Estevou, P. (1999). The diversity of late Neogene sedimentary basins
735 generated by wrench faulting in the Eastern Betic Cordillera, SE Spain. Journal of
736 Petroleum Geology 22. doi: 10.1306/BF9AB7B5-0EB6-11D7-8643000102C1865D.

737 Mora, M. (1993). Tectonic and sedimentary analysis of the Huércal-Overa region, SE Spain, Betic
738 Cordillera, Ph.D. Thesis, Oxford Univ., Oxford, England.

739 Müller, P.D., Roest, W.R. (1992). Fracture Zones in the North Atlantic from Combined Geosat and
740 Seasat Data. Journal of Geophysical Research, 97, 3337-3350.

741

742 Naylor, M.A., Mandl, G., Sijpesteijn, C.H.K. (1986). Fault geometries in basement-induced wrench
743 faulting under different initial stress states. Journal of Structural Geology 8, 737-752.

744 Nicol, A., Cowan, H., Campbell, J., Pettinga J. (1995). Folding and the development of small
745 sedimentary basins along the New Zealand plate boundary. Tectonophysics 241, 47-54.

746 Oldow, J., D'Argenio, B., Ferranti, L., Pappone, G., Marsella, E., Sacchi, M. (1993). Large-scale
747 longitudinal extension in the southern Apennines contractional belt, Italy. Geology 21,
748 1123-1126.

749 Ott d'Estevou, P. and Montenat, C. (1985). Evolution structurale de la zone Betique orientale
750 (Espagne) du Tortonian à l'Holocène. Comptes Rendus de l'Academie des Sciences Paris
751 300, 363-368.

752 Ori G.G. and Friend P.F. (1984). Sedimentary basins, formed and carried piggyback on active thrust
753 sheets, Geology 12 (9) (1984), pp. 475-478.

754 Owens, T.J. and Zandt, G. (1997). Implications of crustal property variations for models of Tibetan
755 plateau evolution. Nature, 387. 37-43.

756 Pedley, R C, Busby, J P, Dabek, Z K. (1993). GRAVMAG User Manual -Interactive 2.5D gravity
757 and magnetic modelling. British Geological Survey, Technical Report WK/93/26/R.

758 Pedrera, A., Marín-Lechado, C., Galindo-Zaldívar, J., Rodríguez-Fernández, L.R. Ruiz-Costan, A.
759 (2006). Fault and fold interaction during the development of the Neogene-Quaternary
760 Almería-Níjar basin (SE Betic Cordilleras). In: G. Moratti, and A. Chalouan (Eds), Tectonic
761 of the Western, Geol. Soc. London. Special Publications 262, 217-230.

762 Pedrera, A., Galindo-Zaldívar, J., Sanz de Galdeano C., and López-Garrido, A.C. (2007). Fold and
763 fault interactions during the development of an elongated narrow basin: the Almanzora
764 Neogene-Quaternary Corridor (SE Betic Cordillera, Spain). Tectonics 26, TC6002,
765 doi:10.1029/ 2007TC002138.

766 Pedrera, A., Galindo-Zaldívar, J., Ruiz-Bustos, A., Rodríguez- Fernández, J., Ruíz-Constán, A.
767 (2009a). The role of small-scale fold and fault development in seismogenic zones: example
768 of the Western Huércal-Overa basin (Eastern Betic Cordillera, Spain). Journal of
769 Quaternary Science 24, 581-592. doi:10.1002/jqs.1246

770 Pedrera, A., Galindo-Zaldívar , J., Ruíz-Constan, A., Duque, C., Marín-Lechado, C., Serrano, I.
771 (2009b). Recent large fold nucleation in the upper crust: Inight from gravity, magnetic,
772 magnetotelluric and seismicity data (Sierra de Los Filabres-Sierra de Las Estancias, Internal
773 Zones, Betic Cordillera). Tectonophysics 463:1-4, 145-160. doi:10.1016/j.tecto2008.09.037

774 Pedrera, A., Pérez-Peña, J. V., Galindo-Zaldívar, J., Azañón, J. M., Azor, A. (2009c). Testing the
775 sensitivity of geomorphic indices in areas of low-rate active folding (eastern Betic
776 Cordillera, Spain). Geomorphology 105, 218-231.

777 Platt, J.P. and Vissers, R.L.M. (1989). Extensional collapse of thickened continental lithosphere: A
778 working hypothesis for the Alboran Sea and Gibraltar Arc. Geology 17, 540-543.

779 Poisson, A. M., Morel, J. L., Andrieux, J., Coulon, M., Wernli, R., Guernet, C. (1999). The origin
780 and development of Neogene basins in the SE Betic Cordillera (SE Spain): a case study of
781 the Tabernas-Sorbas and Huercal Overa Basins. Journal of Petroleum Geology, 22, 97-114.

782 Reading, H.G. (1980). Characteristics and recognition of strike-slip fault systems. In: Balance, P.F.,
783 Reading, H.G. (Eds.), Sedimentation in Oblique-Slip Mobile Zones, Spec. Publ. Int. Ass.
784 Sedim, 7-26.

785 Robinson, E.S. and Çoruh, C. (1988). Basic Exploration Geophysics. Wiley, Chichester.

786 Rosenbaum, G., Lister, G.S., Duboz, C. (2002). Relative motions of Africa, Iberia and Europe
787 during Alpine orogeny. Tectonophysics, 359, 117-129.

788 Rutter, E.H., Maddock, R.H., Hall, S.H., White, S.H. (1986). Comparative microstructures of
789 natural and experimentally produced clay-bearing fault gouges. In: International structure of
790 fault zones, Y. Wang-Chi (Ed.), Pure and Applied Geophysics, 124, 3-30.

791 Shanker D., Kapur N., Singh B. (2002). Normal Fault in contractional tectonics. Journal of the
792 Geological Society, 159, 273-280.

793 Silva, P.G., Goy, J.L., Zazo, C., Lario, J., Bardají, T. (1997). Paleoseismic indicators along
794 'aseismic' fault segments in the Guadalentín depresion (SE Spain). Journal of Geodynamics
795 24, 105-115.

796 Soto, J. I., F. Fernández-Ibáñez, M. Fernàndez, García-Casco, A. (2008). Thermal structure of the
797 crust in the Gibraltar Arc: Influence on active tectonics in the western Mediterranean,
798 *Geochem. Geophys. Geosyst.*, 9, Q10011, doi:10.1029/2008GC002061Stich, D., Ammon,
799 C.J., Morales, J., 2003. Moment tensor solutions for small and moderate earthquakes in the
800 Ibero–Maghreb region. J. Geophys. Res. 108, 2148, doi:10.1029/2002JB002057.

801 Srivastava, S.P., Roest, W.R., Kovacs, L.C., Oakey, G., Levesque, S., Verhoef, J., Macnab, R.
802 (1990). Motion of Iberia since the Late Jurassic: Results from detailed aeromagnetic
803 measurements in the Newfoundland basin. Tecontophysics 184, 229-260.

804 Stich, D., Serpelloni, E., Mancilla, F., Morales, J. (2006). Kinematics of the Iberia-Maghreb plate
805 contact from seismic moment tensors and GPS observations. Tectonophysics, 426, 295-317,
806 doi:10.1016/j.tecto.2006.08.004.

807 Tchalenko, J.S. (1970). Similarities between shear zones of different magnitudes. Geological
808 Society of America Bulletin, 81, 1625-1640.

809 Telford, W.M., Geldart, L.P., Sheriff, R.E. (1990). Applied Geophysics. Cambridge University
810 Press, Cambridge.

811 Van Bemmelen, R.W. (1927). Bijdrage tot de geologie der Betisch Ketens in de provincie Granada.
812 Ph.D. Thesis, Univ. Delft.

813 Vennin, E., Rouchy, J. M., Chaix, C., Blanc-Valleron, M.-M., Caruso, A., Rommevau, V. (2004).
814 Paleoecology constraints on reef-coral morphologies in the Tortonian-early Messinian of
815 the Lorca basin, SE Spain. Palaeogeography, Palaeoclimatology, Palaeoecology, 213, 163-
816 185.

817 Vissers, R.L.M, Platt, J.P., Van der Wal, D. (1995). Late orogenic extension of the Betic Cordillera
818 and the Alboran Domain: A lithospheric view. Tectonics, 14, 786-803.

819 Yin, A. (1993). Mechanics of wedge shaped fault blocks: an elastic solution for contractional
820 wedge. Journal of Geophysical Research, 98. 14245-14256.

821 Zoetemeijer, R., Cloetingh, S., Sassi, W. Roure, F. (1993). Modelling of piggyback-basin
822 stratigraphy: Record of tectonic evolution. Tectonophysics , 226, 253-269.

823

824 **Figure captions**

825

826 Figure 1. Geological setting. (a) Simplified geological map of the Betic Cordillera and (b)
827 enlarged geological map over digital elevation model of the Eastern Betic Cordillera
828 where the locations of the main faults and folds are indicated. The position of
829 Figure 4 is marked. AC: Almanzora Corridor; AMF: Alhama de Murcia Fault; BSB:
830 Bajo Segura Basin; CF: Carboneras Fault; GD: Guadalentín Depression; HOB:
831 Huércal-Overa Basin; PF: Palomares Fault; SCab: Sierra Cabrera; SAlh: Sierra
832 Alhamilla; SAlm: Sierra Almagro; TB: Tabernas Basin; VB: Vera Basin.

Figure 2. Paleostress evolution proposed in previous research for the AMF and surrounding areas.

Figure 3. Stratigraphic sketch of the Huércal-Overa Basin.

Figure 4. Geological map of the Huércal-Overa Basin. The locations of the main faults and folds are indicated. The position of the gravity measurement sites, the outcrops shown in Figures 5 and 6, and the geological cross-sections of Figure 10 are marked. The orientations of small-scale faults are represented in stereographic projection, lower hemisphere ("n=XX" at the bottom right of the plots indicate the number of the faults measured).

Figure 5. Field examples of faults (location indicated in figure 4). (A) Example of WNW-ESE conjugated normal faults with 60º dihedral angle that deform Serravallian-Lower Tortonian conglomerates tilted. (B) NW-SE Normal fault located in the southern boundary of the basin. (C) Detachment parallel to the beds with an associated roll-over in the footwall developed in the succession of conglomerates, sands and grey silts layers. (D) The WNW-ESE Santopetar Fault and their associated roll-over deforming the succession of conglomerates, sands and grey silts. (E) WNW-ESE dextral faults that deform Tortonian sediments.

Figure 6. Field examples of folds (location indicated in figure 4). (A) Example of WNW-ESE antiform that deform Serravallian-Lower Tortonian conglomerates. (B) Northern limb of the WNW-ESE La Parata antiform highly deformed by normal faulting. Note the variation of the dip between the Serravallian-lower Tortonian and the Upper Tortonian sediments. (C) E-W fault-propagation fold deforming the

Quaternary sediments. (D) ENE-WSW to E-W folds succession and related open joints affecting Quaternary sediments. Position of the outcrops marked in figure 4.

Figure 7. Huércal-Overa tectonic map. Kinematic data and paleostress results compiled from our tectonic data and previous studies (Mora, 1993; Augier, 2004; Meijninger, 2006; Pedrera et al., 2007).

Figure 8. Residual gravity anomalies (mGal) and tectonic structures. Note the incidence on the anomaly of the different folds.

Figure 9. 2D models constructed from the residual gravity anomalies that allow us to establish the sedimentary thickness of the basin. Three different gravity models are presented assuming the average, the minimum and the maximum plausible density contrasts. Location in Fig. 8.

Figure 10. Geological cross-sections from structural and gravity data (sedimentary rocks density of 2.35 gr/cm^3). The position is marked in Figure 4.

Figure 11. Evolution of the Huércal-Overa Basin and structural interactions associated with the termination of the Alhama de Murcia Fault.

Table 1 Paleostress determination from microfaults. Measurement sites in Figs. 4 and 7. The main axes orientations are defined by their azimuth and plunge. In addition, the axial ratio values ($R = (\sigma_2 - \sigma_3)/(\sigma_1 - \sigma_3)$) are given for each station.

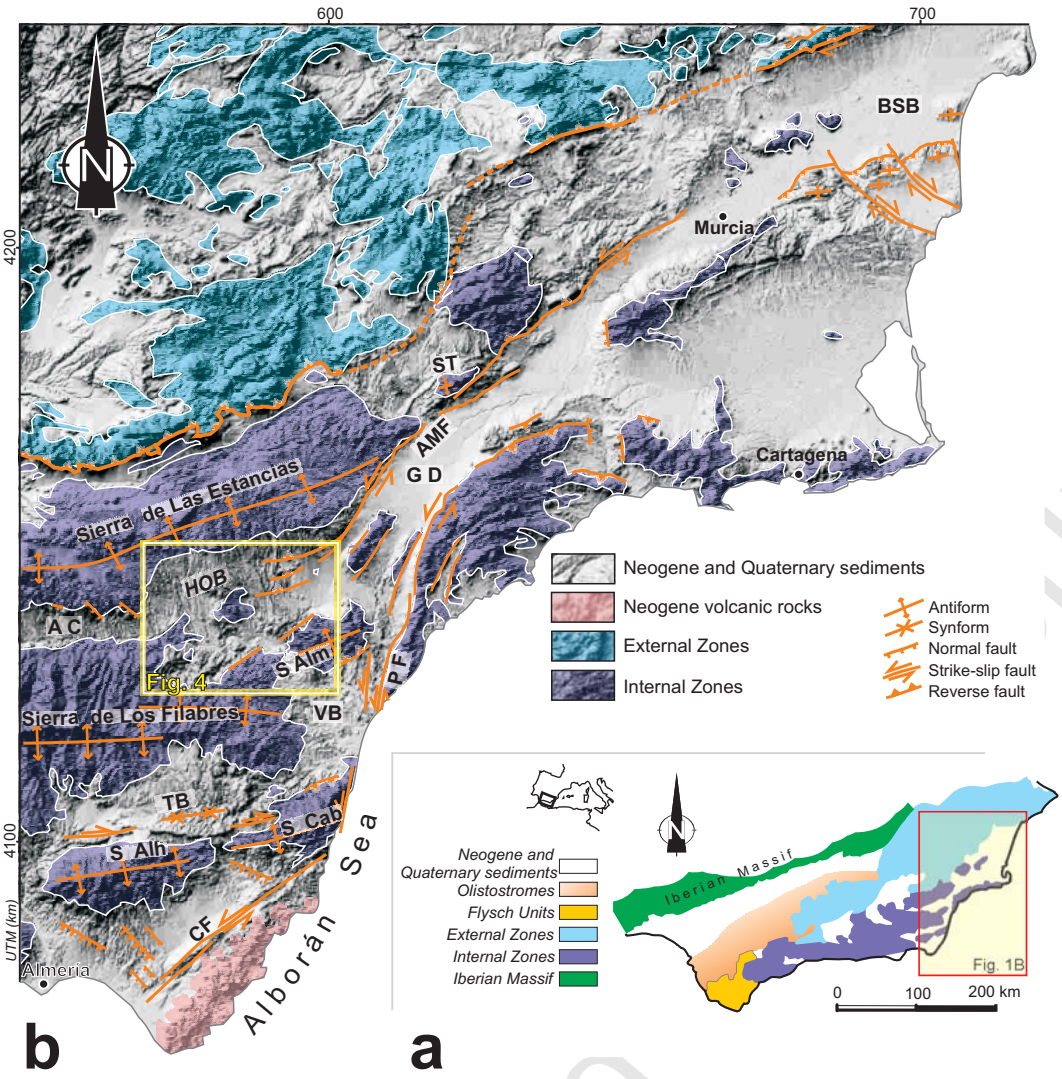

FIG. 1 PEDRERA ET AL. 2009

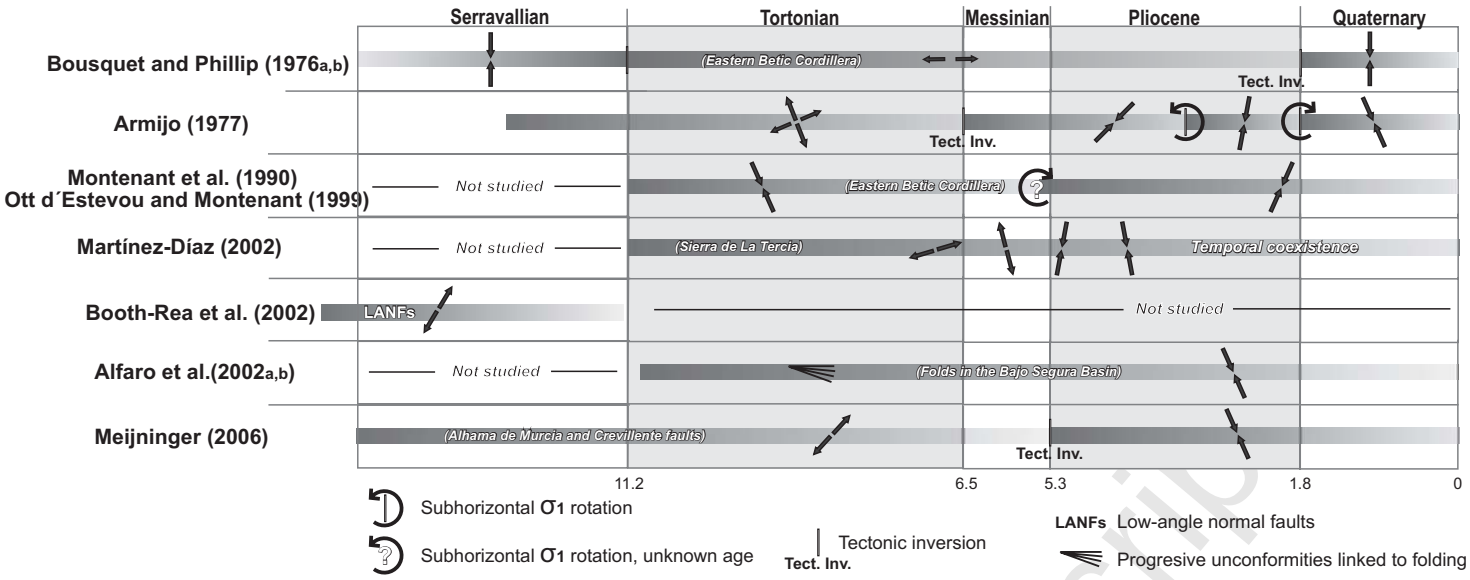

FIG. 2 PEDRERA ET AL. 2009

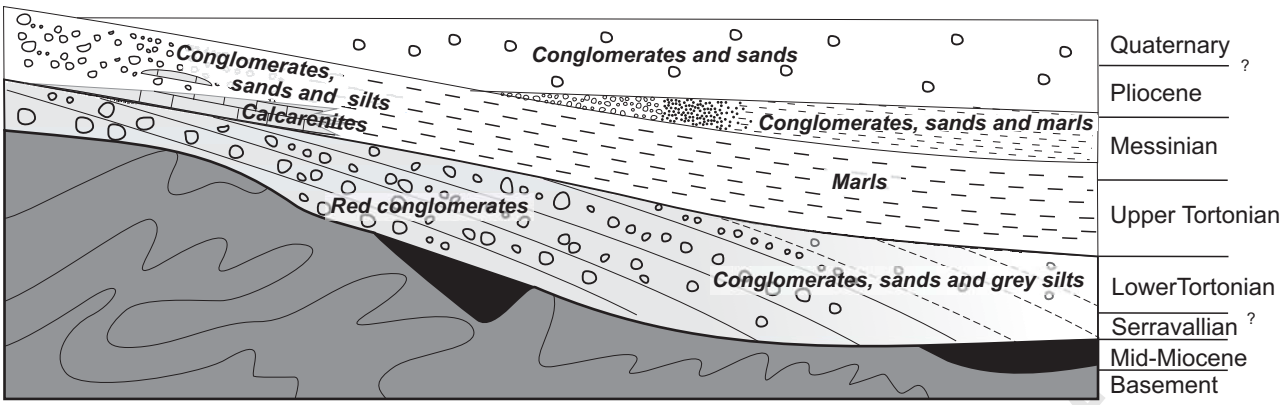

FIG. 3 PEDRERA ET AL. 2009

Figure

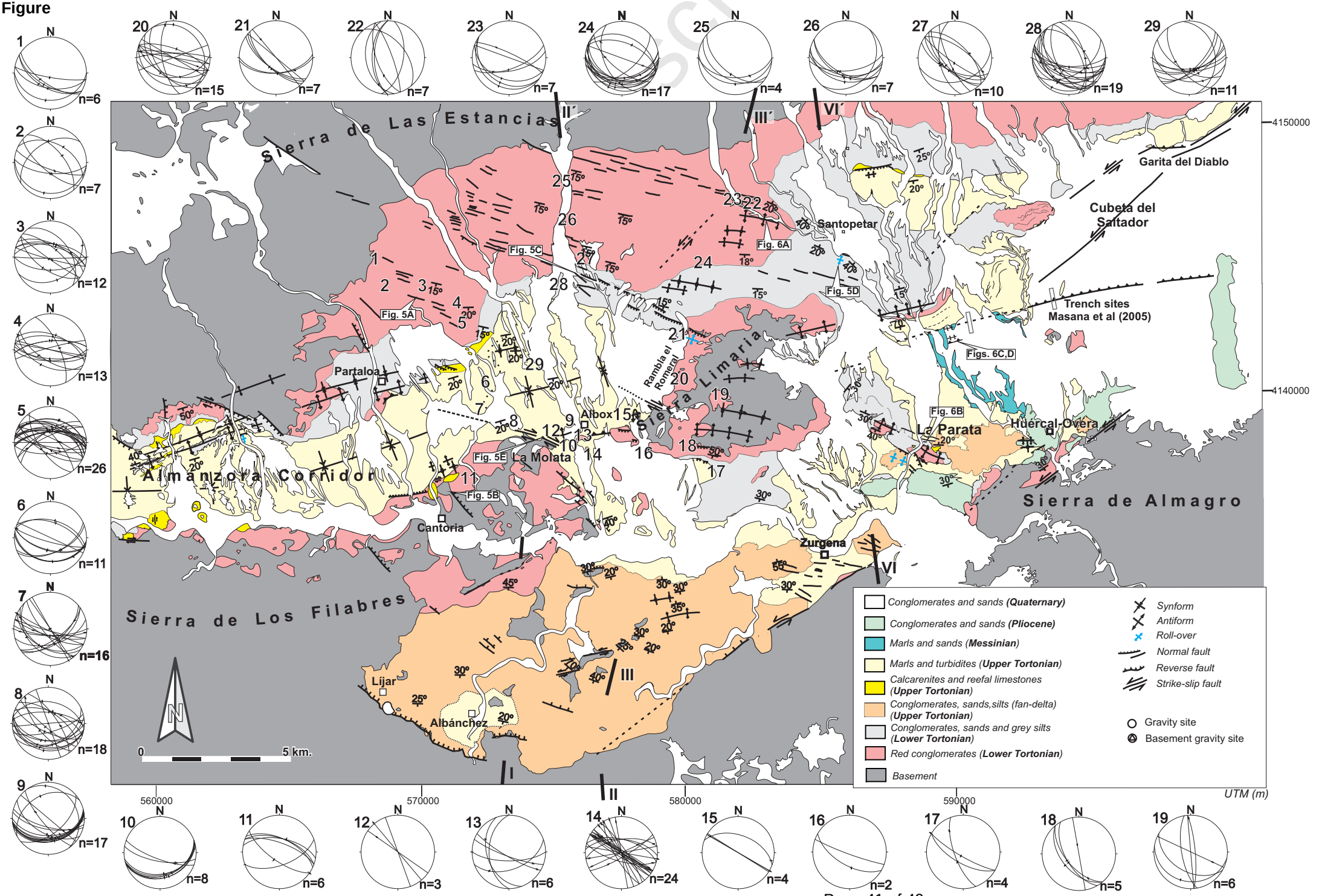

FIG. 4 PEDRERA ET AL. 2008

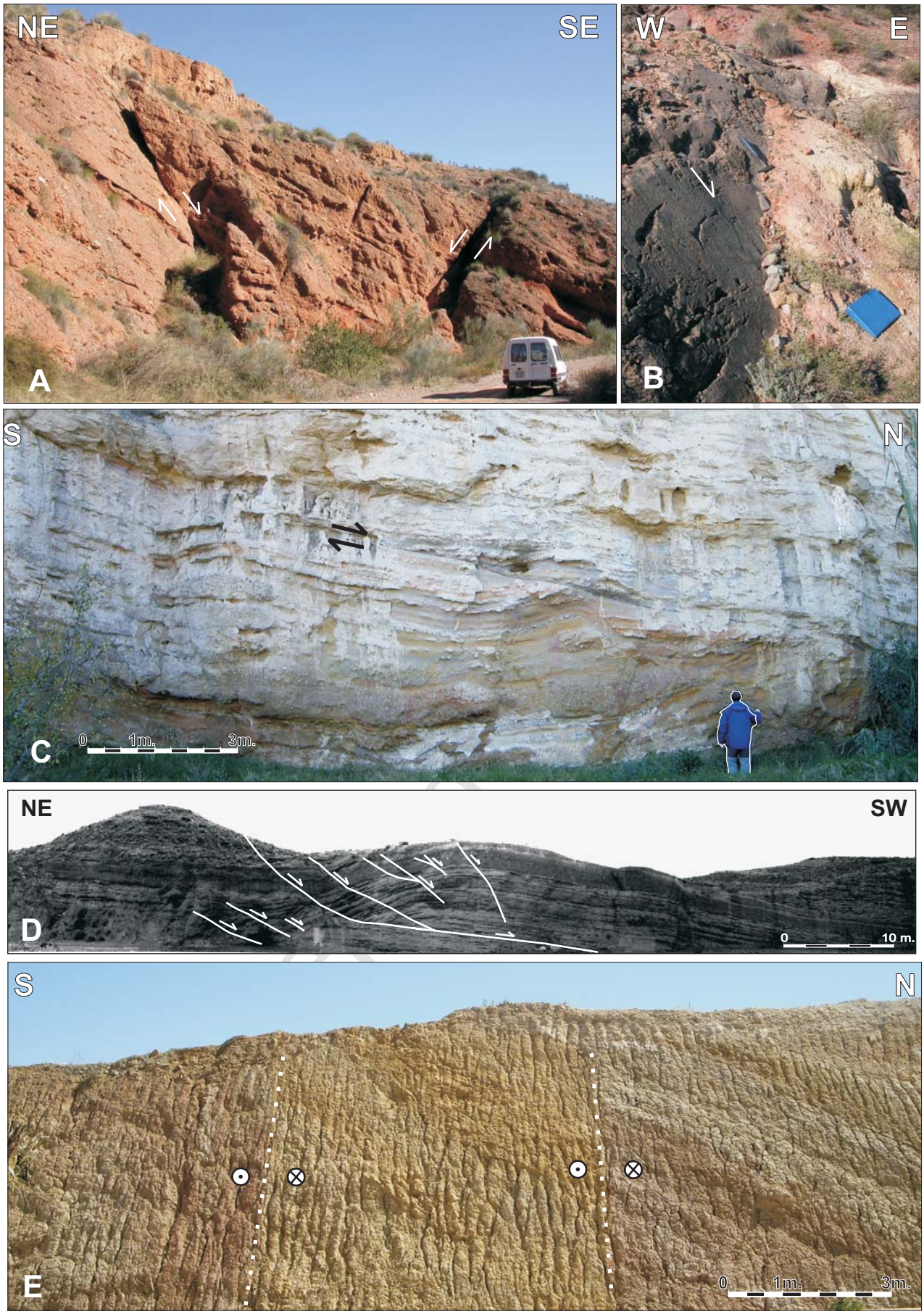

FIG. 5 PEDRERA ET AL. 2008

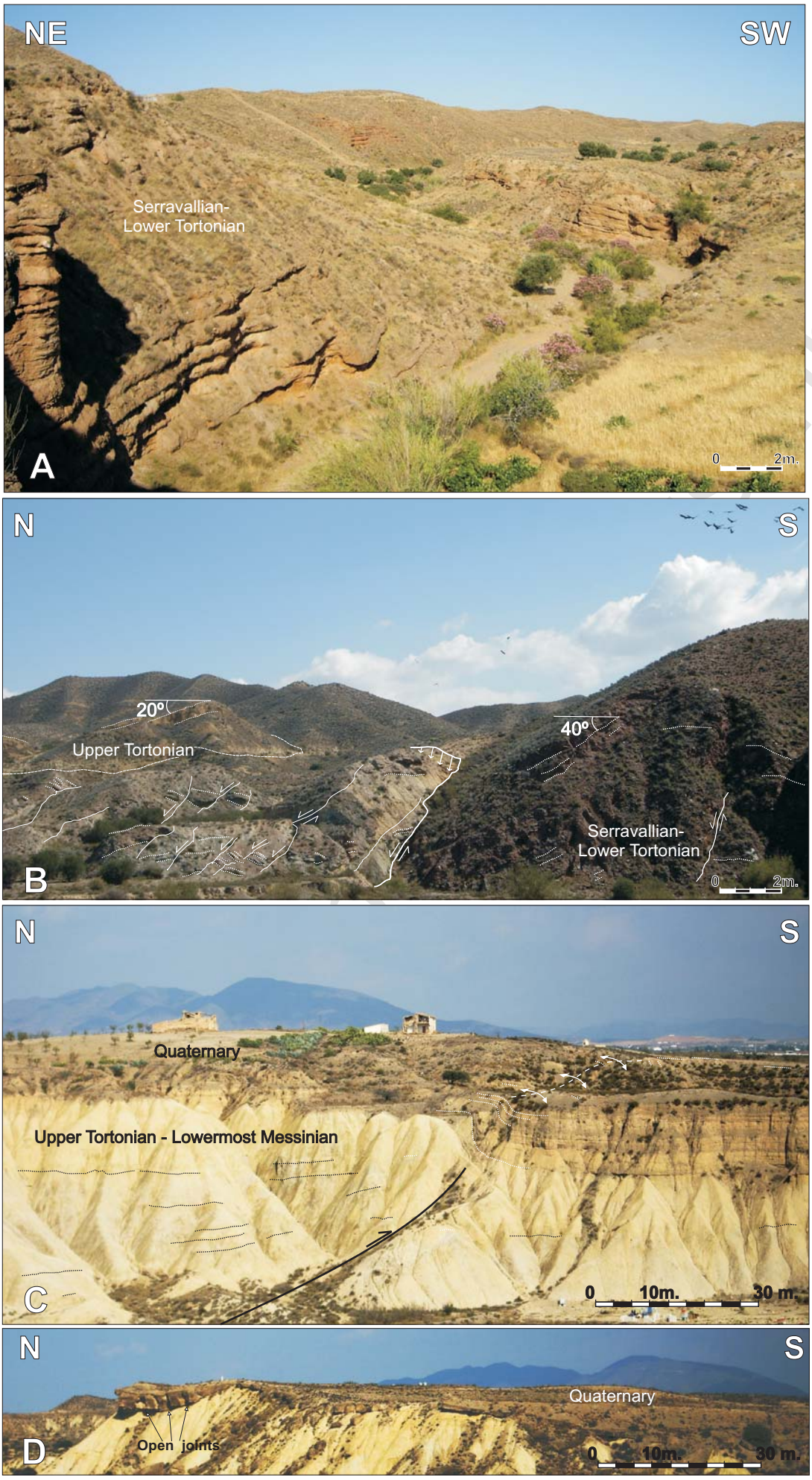

FIG. 6 PEDRERA ET AL. 2008

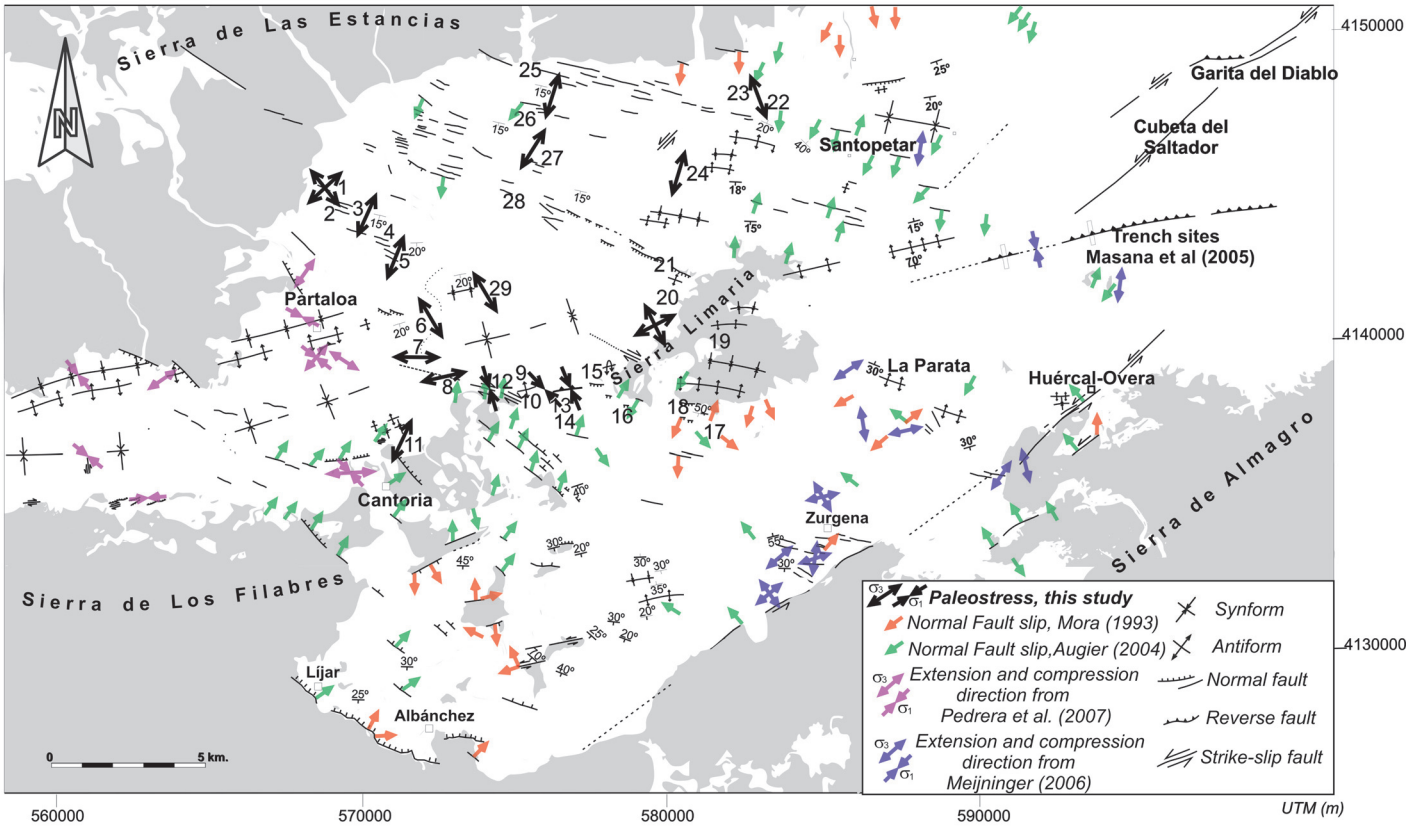

FIG. 7 PEDRERA ET AL. 2009

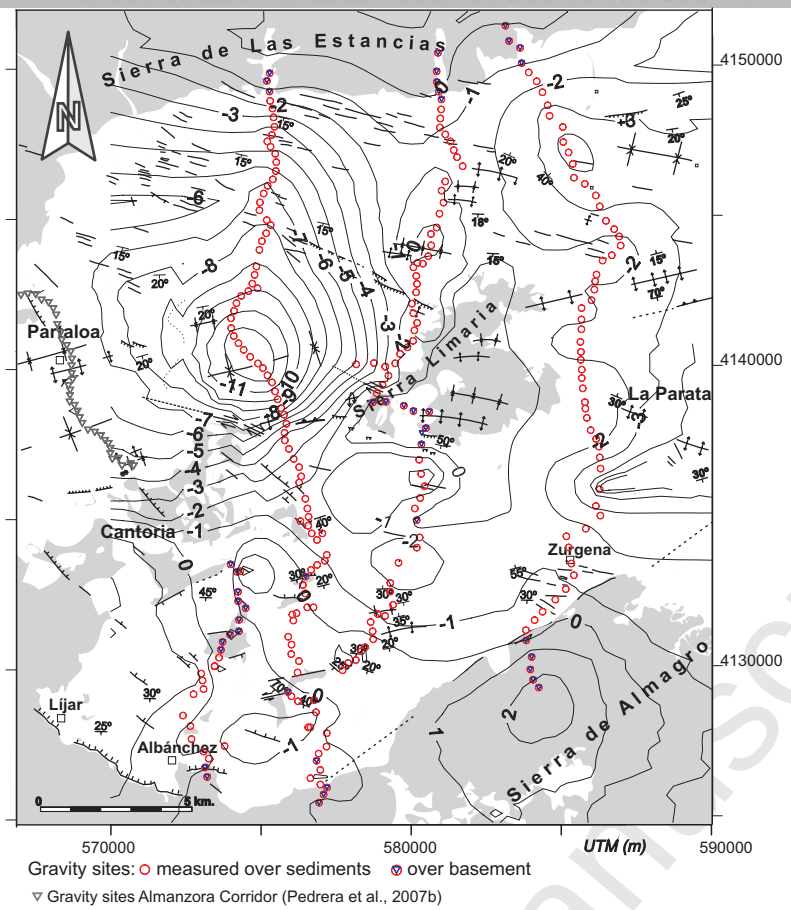

FIG. 8 PEDRERA ET AL. 2009

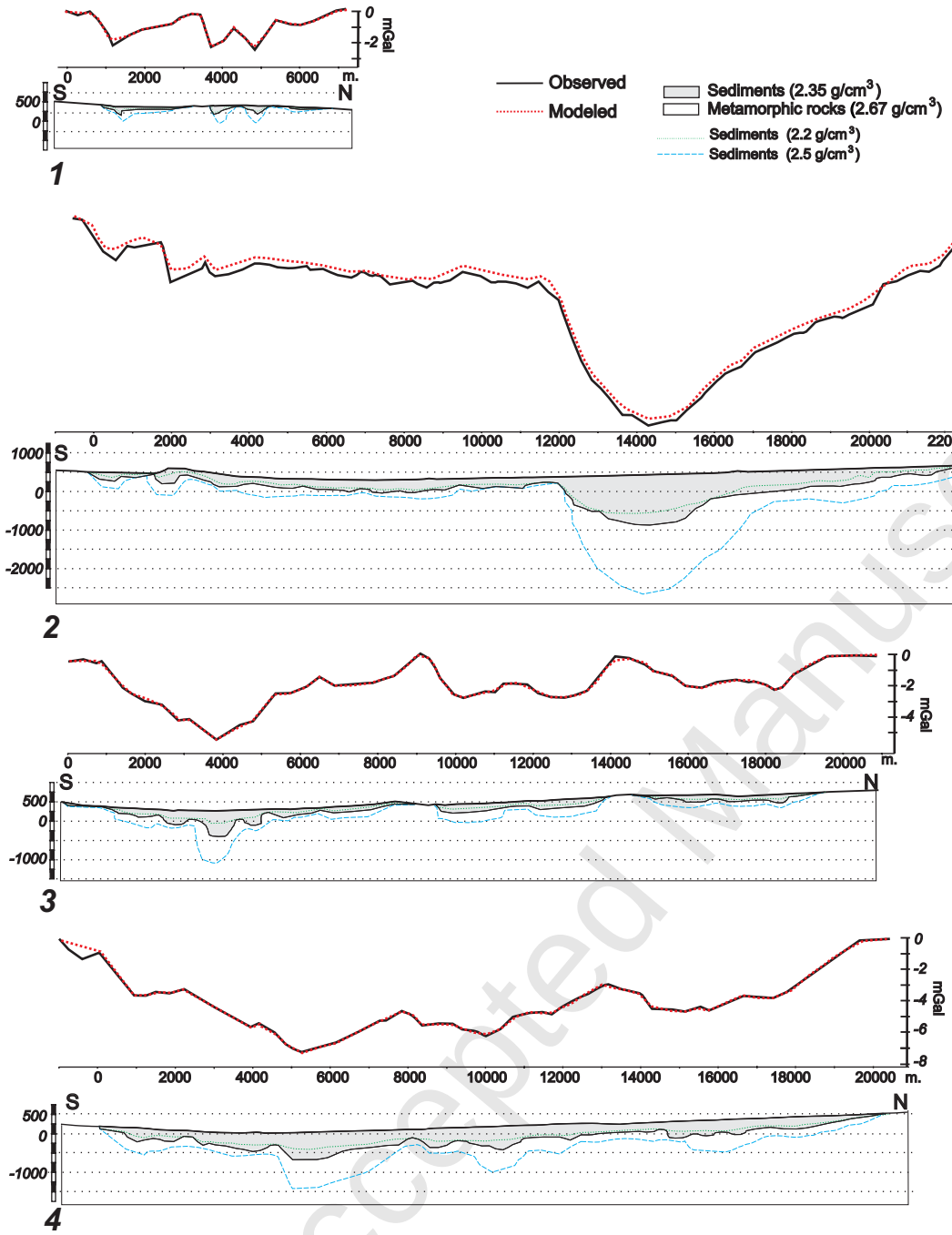

FIG. 9 PEDRERA ET AL. 2008

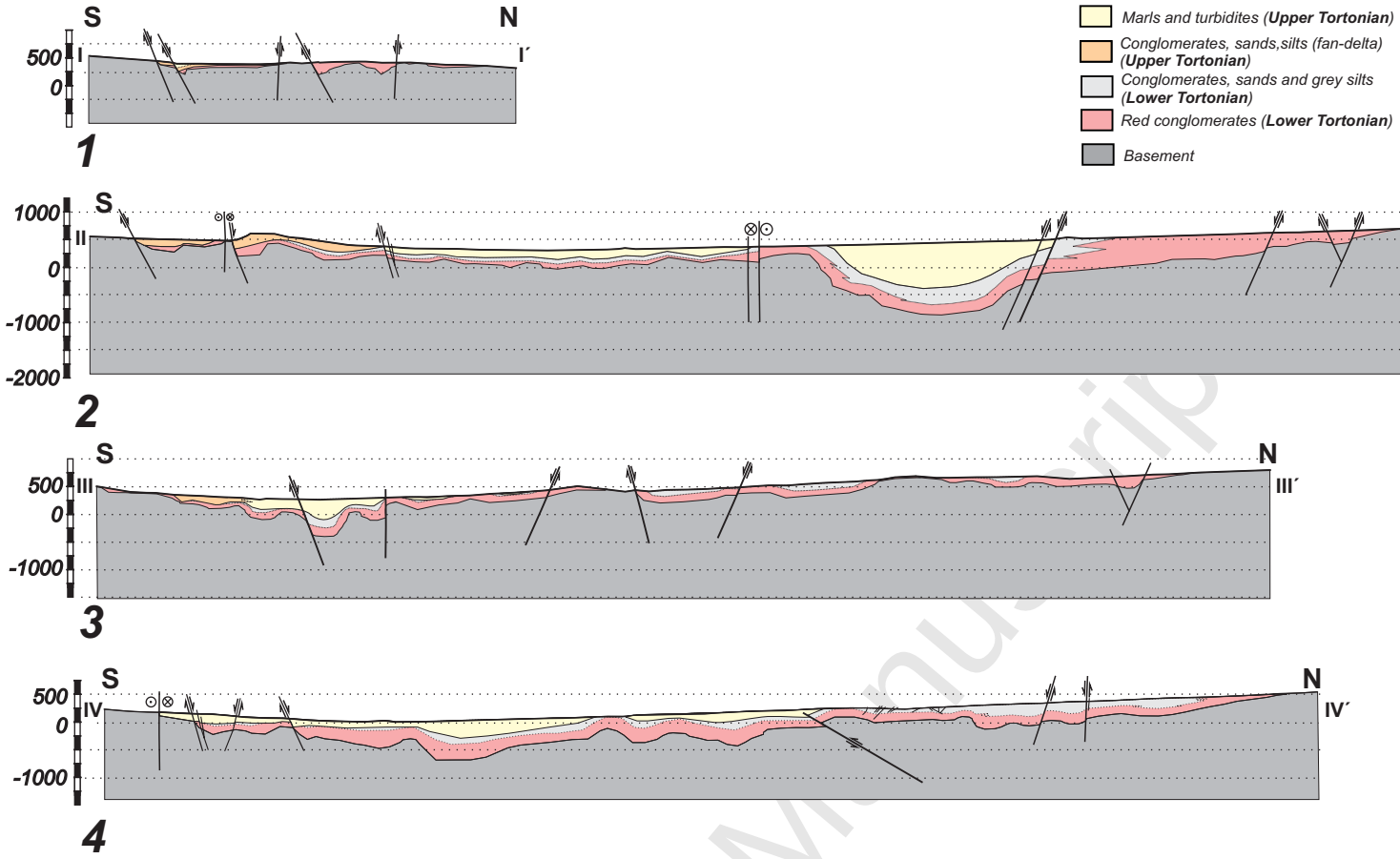

FIG. 10 PEDRERA ET AL. 2009

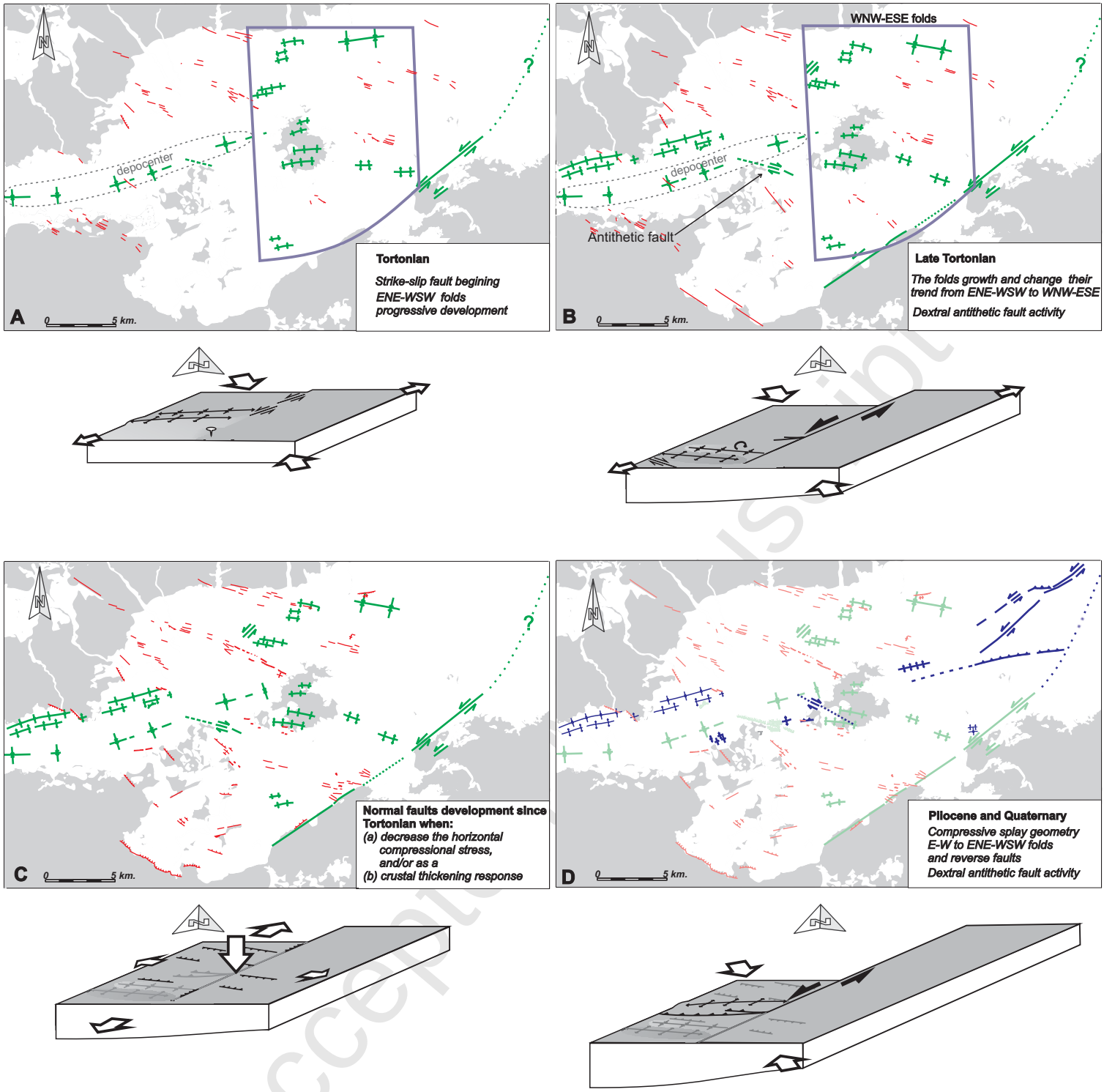

FIG. 11 PEDRERA ET AL. 2009

Outcrop		Data number	Data used	σ_1	σ_2	σ_3	R
1,2 y 3	Serv-L.Tort.	25	22	86º / N183ºE	4º / N336ºE	2º/ N66ºE	0
4	Serv-L.Tort.	14	11	80º / N273ºE	10º / N104ºE	2º/ N14ºE	0.07
5	Serv-L.Tort.	26	18	82º / N163ºE	6º / N28ºE	6º / N297ºE	0.06
6	U. Tort.	11	7	70º / N23ºE	1º / N289ºE	20º / N198ºE	0.21
7	U. Tort.	22	14	86 º/ N207ºE	4º / N360ºE	2º / N90ºE	0.21
			8	76º / N205ºE	13º/ N360º E	6º / N91ºE	0.93
8	U. Tort.	21	17	86º / N174ºE	4º/ N354ºE	0º / N84ºE	0.07
			6	14º / N84ºE	61º / N327ºE	25º / N181ºE	0.25
9	Quat.	17	10	18º / N161ºE	2º / N252ºE	72º / N348ºE	0.35
10	Quat.	8	7	6º / N117ºE	12º / N26ºE	77º / N233ºE	0.56
12	U. Tort.	24	17	8º / N313ºE	48º /N52ºE	41º / N216º	0.07
			6	20º / N184ºE	38º / N78ºE	45º / N296ºE	0.57
17, 18 y 19	Serv-L.Tort.	11	7	23º / N82ºE	6º / N119ºE	6º / N28ºE	0.1
20	Serv-L.Tort.	14	8	12º / N324ºE	76º / N179ºE	8º / N56ºE	0.33
			6	81º / N94ºE	4º / N210ºE	8º / N301ºE	0.23
22	Serv-L.Tort.	11	9	56º / N14ºE	8º / N272ºE	33º / N177ºE	0.69
23	Serv-L.Tort.	19	15	65º / N232ºE	24º / N66ºE	5º / N334ºE	0.08
24	Serv-L.Tort.	10	9	68º / N42ºE	1º / N136ºE	22º / N227ºE	0.56
25 y 26	Serv-L.Tort.	11	9	57º / N202ºE	7º / N101ºE	32º / N7ºE	0
27 y 28	L.Tort.	13	10	80º / N45ºE	10º / N221ºE	1º / N311ºE	0.03
29	U. Tort.	15	12	42º / N200ºE	48º / N20ºE	0º / N110ºE	0.3